MATHEMATICAL MODELING OF GLIOBLASTOMA TUMOR GROWTH UNDER THE INFLUENCE OF CHEMOTHERAPY WITH FLUOROPYRIMIDINE POLYMER F10

A thesis presented to the faculty of the Graduate School of
Western Carolina University in partial fulfillment of the
requirements for the degree of Master of Science in Technology

By
Mitra Shabanisamghabady

Advisor: Dr. Martin L. Tanaka
Department of Engineering & Technology

Committee Members:
Dr. Jeff Lawson, Mathematics and Computer Science Department
Dr. Michael S. June, Department of Engineering & Technology

April 2016

To my family, for their endless support

ACKNOWLEDGEMENTS

TABLE OF CONTENTS

LIST OF TABLES

LIST OF FIGURES

ABSTRACT

MATHEMATICAL MODELING OF GLIOBLASTOMA TUMOR GROWTH UNDER THE INFLUENCE OF CHEMOTHERAPY WITH FLUOROPYRIMIDINE POLYMER F10

Mitra Shabanisamghabady, M.S.T.

Western Carolina University (April 2016)

Director: Dr. Martin L. Tanaka

Glioblastoma multiforme is the most common and most malignant primary tumor of the brain. Optimal therapy results in survival time of 15 months for newly diagnosed cancer and 5-7 months for recurrent disease. Malignant glioblastoma patients demonstrate limited response to conventional therapies that include surgery, radiation, and chemotherapy. New methods of therapy are urgently needed. Mathematical models are often used to understand and describe the behavior of brain tumors. These models can both increase our understanding of tumor growth, as well as aid in the development and preliminary testing of treatment options. In this research five classical cancer growth models, in form of ordinary differential equations (ODEs) were used. These models were exponential, logistic, generalized logistic, Gompertz and Von Bertalanffy growth models. Using data from an in-*vivo* experiment on glioblastoma, and a nonlinear least-squares solver in MATLAB (*lsqcurvefit*), the characteristic parameters of each model were found and then the models were compared to find the best fit. In the second part of the research, using Gompertz model, compartment modeling, in-*vivo* experiment data and *lsqcurvefit* function in MATLAB, the effect of chemotherapy with fluoropyrimidine polymer F10, was modeled. This model can later be used for preliminary testing and treatment options for glioblastomas.

CHAPTER 1: INTRODUCTION

The number of deaths resulting from cancer every year is second only to cardiovascular disease. [1] Primary brain tumors are among the most aggressive and lethal forms of cancer [2] and gliomas are the most prevalent form of these. Gliomas are an important form of brain tumor with high mortality rate. [3] Gliomas are derived from transformed glial cells and account for 30-40% of all primary intracranial neoplasms. [4] The most common and lethal are glioblastoma multiforme (GBM), a World Health Organization grade IV astrocytoma. [5]

Patients diagnosed with glioblastoma have a median survival time of approximately one year despite use of a variety of medical interventions. [6] One reason for this poor prognosis is that GBMs are highly invasive and generate hair-like projections of migratory cells that invade adjacent healthy brain tissue. [3] Glioblastoma is the most common malignant brain tumor and one of the deadliest human malignancies. Optimal therapy results in survival times of 15 months for newly diagnosed cancer and 5–7 months for recurrent disease. New therapeutic modalities are urgently needed. [7]

Mathematical models are useful for studying tumors, because these allow for more logical experimental design and provide valuable insight into the underlying mechanisms of their growth and development.[8] Mathematical models that describe the tumor growth can both increase our understanding of tumor development, as well as aid in the development and preliminary testing of treatment options. [9]

In this research five classical mathematical growth models have been used to model the tumor growth. These models are the Exponential, Logistic, Generalized logistic, Gompertz and Von Bertalanffy models. The solutions for these equations were found either analytically or

numerically. Using the least square curve fitting function (lsqcurvefit) in MATLAB, the models were fitted to the experimental data. The experimental data used for the optimization, came from an in-vivo experiment on nude mice at Wake Forest University. [7] From the optimization the best model among this five models was identified.

In the second part of the research the best model found in the previous part was more developed to model the effect of chemotherapy on tumor growth. The data from this part also came from an in-vivo experiment on nude mice using F10 as the chemotherapy. Three different doses were evaluated and model parameters were obtained. [7]

1.1 Key terms

Apoptosis: A pattern of cell death affecting single cells, marked by shrinkage of the cell, condensation of chromatin, and fragmentation of the cell into membrane-bound bodies that are eliminated by phagocytosis. Often used synonymously with programmed cell death.[10]

Astrocytoma: Astrocytomas are tumors that arise from astrocytes—star-shaped cells that make up the "glue-like" or supportive tissue of the brain.[11]

Chromosome: Chromosomes are thread-like structures located inside the nucleus of animal and plant cells. Each chromosome is made of protein and a single molecule of deoxyribonucleic acid (DNA).[12]

DNA: Deoxyribonucleic acid (DNA) is a long molecule that contains our unique genetic code. Like a recipe book it holds the instructions for making all the proteins in our bodies.[13]

Gene: A gene is the basic physical and functional unit of heredity. Genes, which are made up of DNA, act as instructions to make molecules called proteins.[14]

In vitro: within a glass; observable in a test tube; in an artificial environment.[10]

In vivo: within the living body.[10]

Nude mouse: Inbred strain of laboratory mouse which is hairless and has no thymic tissue. Because it has no source of T lymphocytes, it suffers from a defect in cell-mediated immunity and is highly susceptible to infections. This trait is utilized for immunological studies. Called also athymic mouse.[15]

Orthotopic: Occurring at the normal place.[10]

Proliferation: The reproduction or multiplication of similar forms, especially of cells.[10]

Tumor: neoplasm; a new growth of tissue in which cell multiplication is uncontrolled and progressive.[15]

Xenograft: A graft of tissue transplanted between animals of different species.[15]

CHAPTER 2: LITERATURE REVIEW

2.1 Definition of cancer

Cancer is the name given to a collection of related diseases. In all types of cancer, some of the body's cells begin to divide without stopping and spread into surrounding tissues.[16] Cancer is the uncontrolled growth of abnormal cells in the body.[17] Cancer can start almost anywhere in the human body, which is made up of trillions of cells.[16]

Normally, human cells grow and divide to form new cells as the body needs them. When cells grow old or become damaged, they die, and new cells take their place.[16] Tumors are created by cells that have lost the ability to assemble and create tissues of normal form and function. The disease is generally named by the type of malfunctioning cells. Some tumors grow fast at the beginning and then stop. These are called benign tumors. In contrast, cancerous tumors do not stop growing and are called malignant tumors.[18]

Cancer cells differ from normal cells in many ways that allow them to grow out of control and become invasive.[16] Some cancerous cells have the ability to proliferate indefinitely (immortalization)[16, 18]. They may also they have the ability to grow without attachment to solid substrate (anchorage independence).[18] In addition, cancer cells may be able to ignore signals that normally tell cells to stop dividing or signal to begin the process of apoptosis (programmed cell death) which the body uses to eliminate unneeded cells. Cancer cells may be able to influence the normal cells, molecules, and blood vessels that surround and feed a tumor—an area known as the microenvironment. For instance, cancer cells can induce nearby normal cells to form blood vessels (angiogenesis) that supply tumors with oxygen and nutrients, which the tumor needs to grow. These blood vessels also remove waste products from tumors.[16]

2.2 How cancer arises

Somatic mutations are alterations in DNA that occur after conception. These can occur in any of the cells of the body except the germ cells (sperm and egg) and therefore are not passed on to children. These alterations can, but do not always, cause cancer.[19] Mutant cells can turn into cancerous cells. In a mutant cells the loss of entire chromosomes, presence of extra copies of other chromosomes or the fusion of the arm of one chromosome with part of another can be seen.[18]

The genetic changes that contribute to cancer tend to affect three main types of genes, proto-oncogenes, tumor suppressor genes, and DNA repair genes. These changes are sometimes called "drivers" of cancer. Proto-oncogenes are involved in normal cell growth and division. However, when these genes are altered in certain ways or are more active than normal, they may become cancer-causing genes (oncogenes), allowing cells to grow and survive when they should not. Tumor suppressor genes are also involved in controlling cell growth and division. Cells with certain alterations in tumor suppressor genes may divide in an uncontrolled manner. DNA repair genes are responsible for in fixing damaged DNA. Cells with mutations in these genes tend to result in additional mutations in other genes. Together, these mutations may cause cells to become cancerous.[16]

The cause of cancer has not been found for all cancers but for some cancers heredity and environment play a role.[18] Cancer causing environmental exposures include substances, such as the chemicals in tobacco smoke, and radiation, such as ultraviolet rays from the sun.[16]

5

2.3 Glioblastoma

Glioblastomas are tumors that arise from astrocytes, the star-shaped cells that make up the "glue-like" supportive tissue of the brain (Figure 2.1). These tumors are usually highly malignant (cancerous) because the cells reproduce quickly and are supported by a large network of blood vessels. Glioblastomas are generally found in the cerebral hemispheres of the brain, but can be found anywhere in the brain or spinal cord. This type of tumor represents about 17% of all primary brain tumors. Primary tumors starts at the brain itself. They increase in frequency with age, and affect more men than women. Only three percent of childhood brain tumors are glioblastomas.[20]
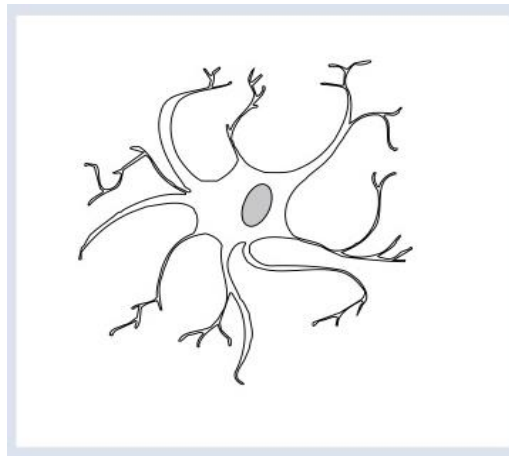
Figure 2.1 Astrocytes [11]

Glioblastoma is the most common malignant brain tumor and one of the deadliest human malignancies. [7,21,22] Optimal therapy results in survival times of 15 months for newly diagnosed cancer and 5–7 months for recurrent disease. New therapeutic modalities are urgently needed.[7]

These tumors are "graded" on a scale from I to IV based on how normal or abnormal the cells look. There are low-grade astrocytomas and high-grade astrocytomas. Low-grade

astrocytomas are usually localized and grow slowly. High-grade astrocytomas grow at a rapid pace and require a different course of treatment. Most astrocytoma tumors in children are low grade. In adults, the majority are high grade.[23] Glioblastoma multiforme (GBM) is a World Health Organization grade IV astrocytoma.[5]

2.4 Cancer treatment

Treatment options depend on the type of cancer, its stage, if the cancer has spread, and your general health. The goal of treatment is to kill as many cancerous cells while minimizing damage to normal cells nearby.[17] The most common treatments for cancer are surgery, chemotherapy, and radiation.[17, 24] Surgery can be used to take out the cancer. The surgeon might also take out some or all of the body part the cancer affects. Chemotherapy is the use of drugs to kill cancer cells or slow their growth. Some chemo can be given by IV (into a vein through a needle), and others are in the form of a pill you swallow. Because chemotherapeutic drugs travel to nearly all parts of the body, they are useful for cancer that has spread. Radiation is also used to kill or slow the growth of cancer cells. Its effect is localized and it can be used alone or with surgery and/or chemotherapy.[24]

2.5 Cancer treatment with F10

Many different drugs are used for chemotherapy and new drugs are being developed. One group of substances used to treat cancer are flouropyrimidine and its polymers. A flouropyrimidine is a type of antimetabolite.[25] Antimetabolites are drugs that interfere with one or more enzymes or their reactions that are necessary for DNA synthesis. They affect DNA synthesis by acting as a substitute to the actual metabolites that would be used in normal metabolism.[26]

One of the polymers of flouropyrimidine is F10. F10 is a polymer of 5-fluoro-2′-deoxyuridine-5′-O-monophosphate (FdUMP), the thymidylate synthase (TS) inhibitory metabolite of 5-fluorouracil (5-FU). Thymidylate synthase is the enzyme responsible for the conversion by methylation of deoxyuridine monophosphate, dUMP, to thymidine monophosphate. Thymidine monophosphase is a deoxyribose called either TMP or dTMP which after conversion into thymidine triphosphate, TTP, is incorporated in DNA.[27] F10 is a novel anti-tumor agent with minimal systemic toxicity in vivo and strong cytotoxicity towards glioblastoma (GBM) cells in vitro. In addition, because F10 also displays strong efficacy for GBM treatment with minimal toxicity in nude mice, it a promising drug-candidate for treating GBM in human patients.[7]
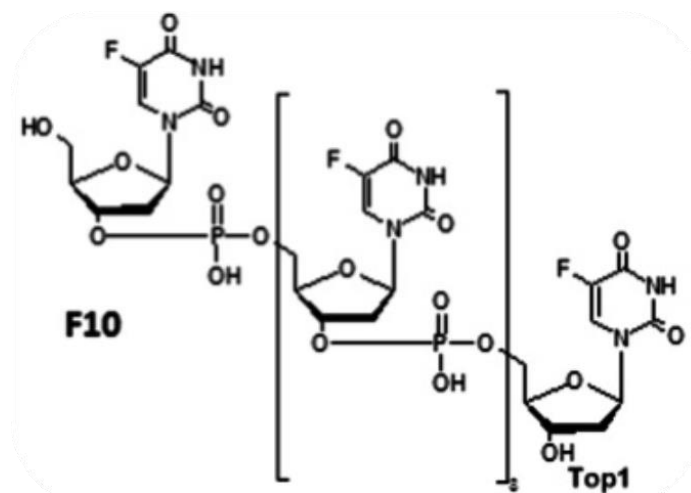
Figure 2.2 Chemical Structure of F10 [7]

2.6 Mathematical models

Mathematical modeling is a powerful tool for analyzing biological problems that allows one to develop and test hypotheses which can lead to a better understanding of the biological process. The essentials of a realistic and useful model are

(i) a sound understanding and appreciation of the biological problem

(ii) a realistic mathematical representation of the important biological phenomena

(iii) useful solutions, preferably quantitative, to what is crucially important

(iv) a biological interpretation of the mathematical results in terms of insights and predictions. The mathematics is dictated by the biology and not vice-versa.[28, 29]

Mathematical models are often used to understand and predict the behavior of brain tumors.[3] Mathematical models that describe the tumor development and growth can both increase our understanding of tumor behavior, as well as aid in the development and preliminary testing of treatment options. These models can provide insight into the vulnerability of different types of tumors to different anti-angiogenic drugs, suggesting avenues for the development of new treatment regimes. They also provide a quantitative framework to determine tumor prognosis.[8]
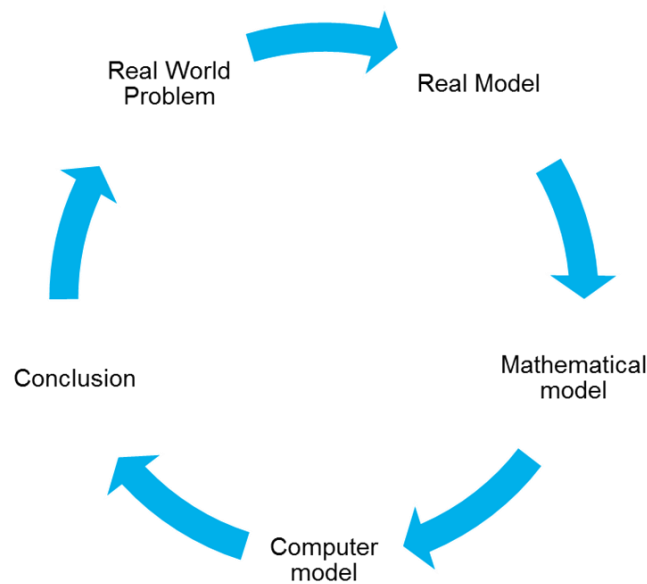
Figure 2.3 Mathematical Modeling Steps

2.7 Mathematical models for tumor growth

Over the last few decades increasingly complex mathematical models for cancerous growth have been developed.[9] There are different groups of models used for modeling tumor growth and each of them has advantages and disadvantages.

Discrete models

Discrete models are able to incorporate parameters and biological rules discovered from cellular research. For a 10 μm glioblastoma cell diameter, cell populations can reach 200 billion by the time the body of a tumor reaches 3 cm. This is the diameter in which GBMs are often first detected.[28] Discrete modeling of 200 billion individual units is beyond the capability of most computers. Therefore these models can only be used for extremely small developing tumors.[3]

Continuum model

Continuum models consider tumors as spatial distributions of cell densities. As a result, the computational requirements are substantially reduced allowing tumors of clinically significant size to be modeled.[30, 31] However, since continuum models do not consider cells individually, they lack the capability to simulate cell-to-cell interactions.[3]

Compartment model

In a compartment model, cells are grouped based on phenotype and level of differentiation. Such models are effective at describing how the sub-populations of various types of cells grow. These models are computationally efficient and can handle many different types of cells.[3]

2.8 Classical tumor growth models

For many decades mathematical models have been used to model tumor growth. In this part five classical mathematical models in form of ordinary differential equations have been

introduced. These models are the Exponential, Logistic, Generalized logistic, Gompertz and Von Bertalanffy models.

Exponential growth model

The exponential growth model is the simplest model that can be used to model tumor growth. This model describes growth of a population which its growth is proportional to its size. The ordinary differential equation for this model is,

$$\frac{dx(t)}{dt} = ax(t), \text{(2.1)}$$

where x is the population size, t is time and a is the growth rate.

The exponential model has been used to model benign tumors and malignant tumors in their early stages. This model has been used first in the research of tumor growth modeling by Collins et al.[32] and Kusama et al.[33]. Later the general assumption that tumor cells grow exponentially has been used in other cancer modeling research.[34, 35] The model kinetics agree with the unlimited proliferative activity of tumor cells recorded in early, mainly in vitro, studies.[36]

Logistic, generalized logistic and Gompertz growth model

Logistic growth describes the growth of a population where its population cannot exceed a certain amount because of the environment limitations. The ordinary differential equation for this model is,

$$\frac{dx(t)}{dt} = ax(t)\left(1 - \frac{x(t)}{K}\right), \text{(2.2)}$$

where, x is the population size, t is time, a is the growth rate and K is the population maximum possible size due to the environment limits.

The generalized logistic function or curve, also known as Richards' curve is an extension of the logistic or sigmoid functions that allows for more flexible S-shaped curves. The ordinary differential equation for this model is,

$$\frac{dx(t)}{dt} = ax(t)(1 - (\frac{x(t)}{K})^v),$$

(2.3)

where, x is the population size, t is time, a is the growth rate, K is the population maximum possible size due to the environment limits also known as the carrying capacity and v affects how smooth the curve is approaching the carrying capacity. The logistic model has been used to describe tumor growth [37] while others have used the generalized logistic model [38].

When a different parameterization is employed, the generalized logistic model converges when $v \to 0$, to the Gompertz model, [35] define by

$$\frac{dx(t)}{dt} = ae^{-\beta t}x(t),$$

(2.4)

where, x is the population size, t is time, a is the initial proliferation rate and β is the rate exponential decay of this proliferation rate. This model was first used in modeling tumor growth in [39] and later in [40].

Von Bertalanffy

The Von Bertalanffy model proposed to derive general laws of organic growth. Stating that the net growth rate should result from the balance of synthesis and destruction.[35] The ordinary differential equation for this model is,

$$\frac{dx(t)}{dt} = ax(t)^\gamma - bx(t),$$

(2.5)

where, x is the population size, t is time, a is the growth rate, and b is the destruction rate.

CHAPTER 3: MODELING THE NATURAL GLIOBLASTOMA GROWTH

3.1 In-vivo mice experiment

The data used for this research was obtained from an experiment performed by Dr. Waldemar Debinski, M.D., Ph.D. and his research group at the Brain Tumor Center of Excellence, Wake Forest University School of Medicine. In this experiment, the cytotoxicity of F10 towards glioblastoma cells was investigated and the anti-tumor activity of locally administered F10 towards an orthotopic xenograft model of glioblastoma was evaluated [7]. The data used in this research is from the orthotopic xenograft model of GBM part of the experiment.

The animal experiments were performed in accordance with protocols approved by Wake Forest School of Medicine Animal Care and Use Committee in accordance with National Institutes of Health guidelines. G48a cells were injected into the deep white matter of the posterior thalamus of nude mice (7-week old). A total volume of 5 μL was injected over a 5 min period. There were four groups of animals in four different cages. In each cage there were 5 mice. The first group of mice did not go under any kind of treatment. But the mice in the 3 other cages were treated with F10 at concentrations (80, 120 and 160 mg/kg) for a duration of 7 days with the first treatment beginning 21 days after the tumor cell implantation.

The tumor growth was monitored by evaluating bioluminescence using IVIS imaging system three times after the tumor cell implantation. Bioluminescence imaging uses the same enzyme and substrate that fireflies use to generate light to track of cells within small animals. The enzyme, luciferase, can be inserted into the genome of cancer cells. These cells are then implanted within mice, and a tail vein (intra-peritoneal) injection of luciferin delivers the substrate to the cells. The combination of luciferin and luciferase causes light to be emitted, this

light can then be captured using a sensitive camera. Measurement are taken with the mouse supported on a heated stage in an enclosed, light-tight box.[41]
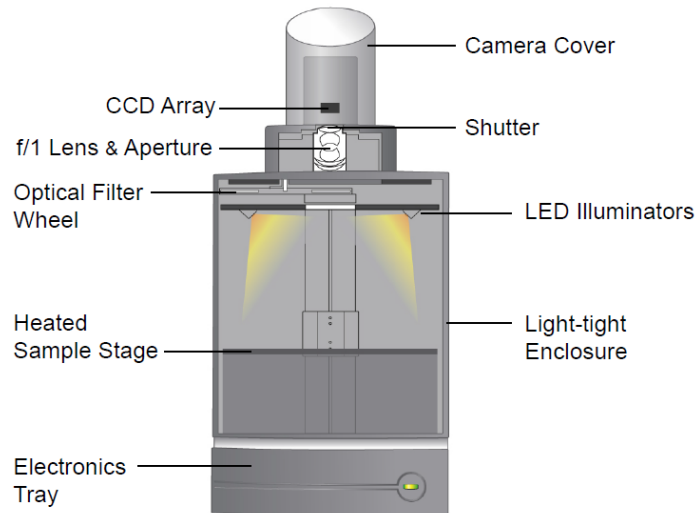
Figure 3.1 The IVIS® Imaging Chamber [42]

A part of the IVIS imaging result can be seen in Figure 3.2. Vehicle treated shown in the figure is the same as no treatment. For more information on this in-vivo mice experiment refer to [7].
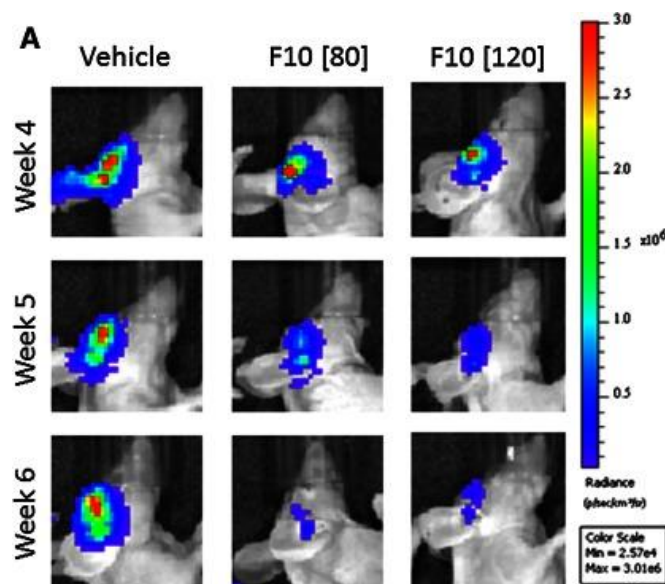
Figure 3.2 Luciferase Signal from F10- and Vehicle-Treated Nude Mice at 80 and 120 mg/kg Doses [7]

3.2 Extraction and analysis of raw data

This research was performed in collaboration with Dr. Debinski's research group at Wake Forest University, we had access to the data that had not yet been published. Data from cage 1 is presented in tables 3.1. Mice in cage 1 were vehicle treated 21 days after the tumor implantation till day 28. Vehicle treatment doesn't affect the tumor cells and it is the same as no treatment.

Table 3.1 In-Vivo Mice Experiment Data from Cage One

ROI	Total Flux [p/s]	Date and Time	Time Point
ROI 1	8.33E+05	3/26/2011 9:09	Week 4
ROI 2	4.22E+06	3/26/2011 9:09	Week 4
ROI 3	1.84E+07	3/26/2011 9:09	Week 4
ROI 4	1.38E+06	3/26/2011 9:09	Week 4
ROI 5	3.02E+06	3/26/2011 9:09	Week 4
ROI 1	6.27E+06	4/1/2011 18:54	Week 5
ROI 2	7.38E+07	4/1/2011 18:54	Week 5
ROI 3	1.13E+06	4/1/2011 18:54	Week 5
ROI 1	2.50E+07	4/9/2011 16:04	Week 6
ROI 2	3.93E+08	4/9/2011 16:04	Week 6
ROI 3	6.67E+06	4/9/2011 16:04	Week 6

Initially there were five mice in cage 1. ROI (region of interest) refers to each mice in the imaging chamber. Imaging was performed on each mouse 3 times after the tumor implantation, at weeks 4, 5 and 6. However, mice 4 and 5 were sacrificed after week 4, so there is no imaging data for weeks 5 and 6 for these mice. The data are shown as the total flux in photons per second.

First, the data points in photons per second versus time in day were plotted in to get a general idea of how the photon emission changed over time. Table 3.2 and figure 3.3 show the data from mouse 1 in cage 1:

Table 3.2 In-Vivo Mice Experiment Data for Cage One Mouse One

ROI	Total Flux [p/s]	Date and Time	Group	Time Point
ROI 1	8.33E+05	3/26/2011 9:09	Cage 1	Week 4
ROI 1	6.27E+06	4/1/2011 18:54	Cage 1	Week 5
ROI 1	2.50E+07	4/9/2011 16:04	Cage 1	Week 6
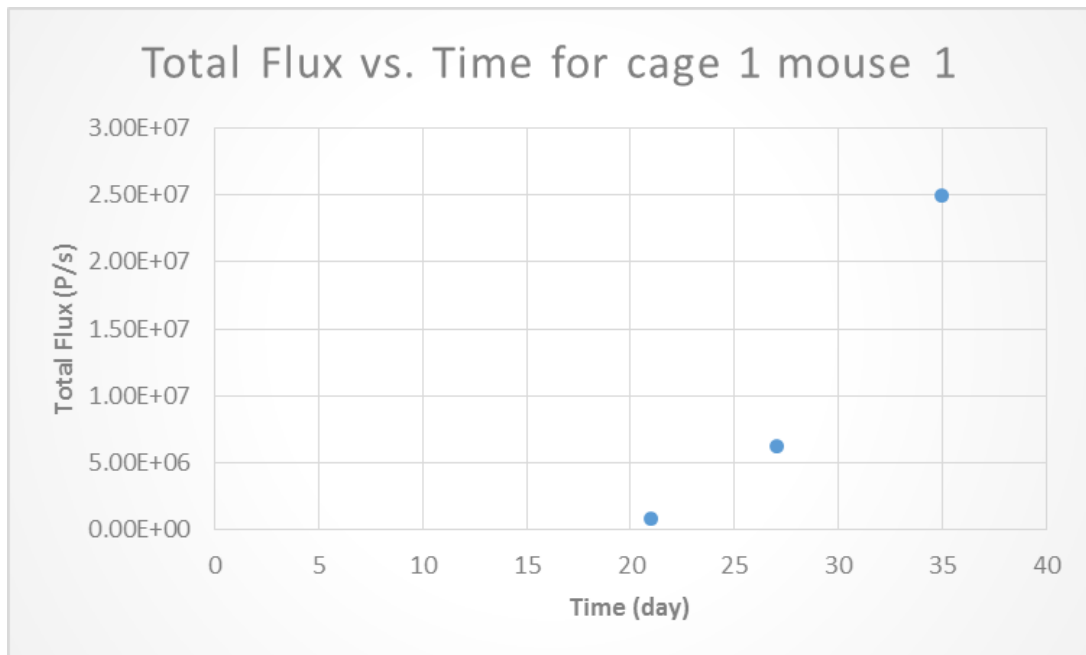
Figure 3.3 Total Flux vs. Time for Cage One Mouse One

It can be seen from the table and the graph that the photon emission and therefore the volume of the tumor increased as time passed. In addition, the rate of growth was also observed to increase. Analysis of mouse 2 data yielded similar results (Table 3.3 & Figure 3.4).

Table 3.3 In-Vivo Mice Experiment Data from Cage One Mouse Two

ROI	Total Flux [p/s]	Date and Time	Group	Time Point
ROI 2	4.22E+06	3/26/2011 9:09	Cage 1	Week 4
ROI 2	7.38E+07	4/1/2011 18:54	Cage 1	Week 5
ROI 2	3.93E+08	4/9/2011 16:04	Cage 1	Week 6
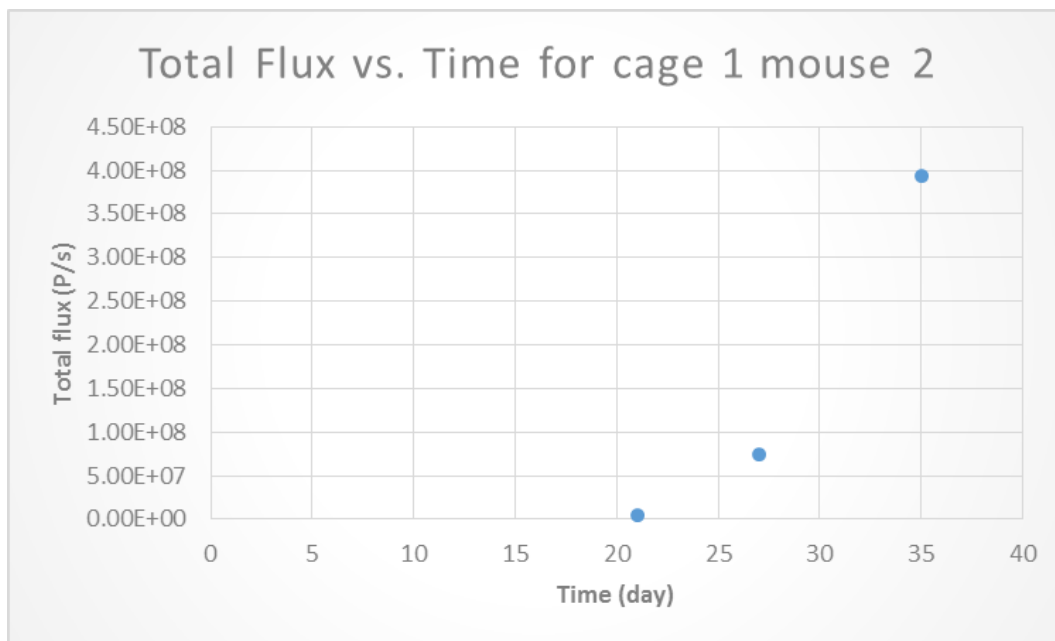
Figure 3.4 Total Flux vs. Time from Cage One Mouse Two

Table 3.4 and figure 3.5 show the data from mouse 3 in cage 1:

Table 3.4 In-Vivo Mice Experiment Data from Cage One Mouse Three

ROI	Total Flux [p/s]	Date and Time	Group	Time Point
ROI 3	1.84E+07	3/26/2011 9:09	Cage 1	Week 4
ROI 3	1.13E+06	4/1/2011 18:54	Cage 1	Week 5
ROI 3	6.67E+06	4/9/2011 16:04	Cage 1	Week 6
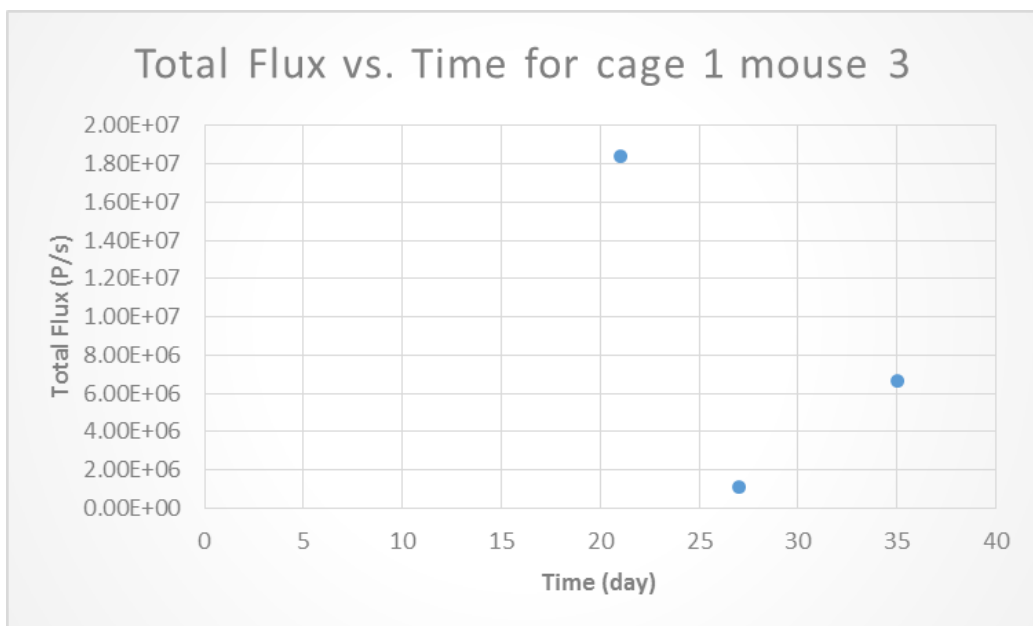
Figure 3.5 Total Flux vs. Time from Cage One Mouse Three

As shown in Figure 3.5, tumor growth in mouse 3 from cage 1 is not normal. Mouse 3 from cage 1 was not experiencing any form of treatment after the tumor implantation so the photon emission was expected to increase. Photon emission and therefore the volume of the tumor for mouse 3 decreased from day 21 to day 27 without any clear reason and therefore data from mouse 3 was eliminated from the data analysis.

Because mice 4 and 5 from cage 1 were sacrifices there was insufficient data to track tumor growth for these mice. Table 3.5 and figure 3.6 show the data from cage 1 mice 1, 2 and 4 averaged:

Table 3.5 In-Vivo Mice Experiment Averaged Data from Cage One

Averaged Total Flux [p/s]	Date and Time	Group	Time Point
2.36E+06	3/26/2011 9:09	Cage 1	Week 4
4.00E+07	4/1/2011 18:54	Cage 1	Week 5
2.09E+08	4/9/2011 16:04	Cage 1	Week 6
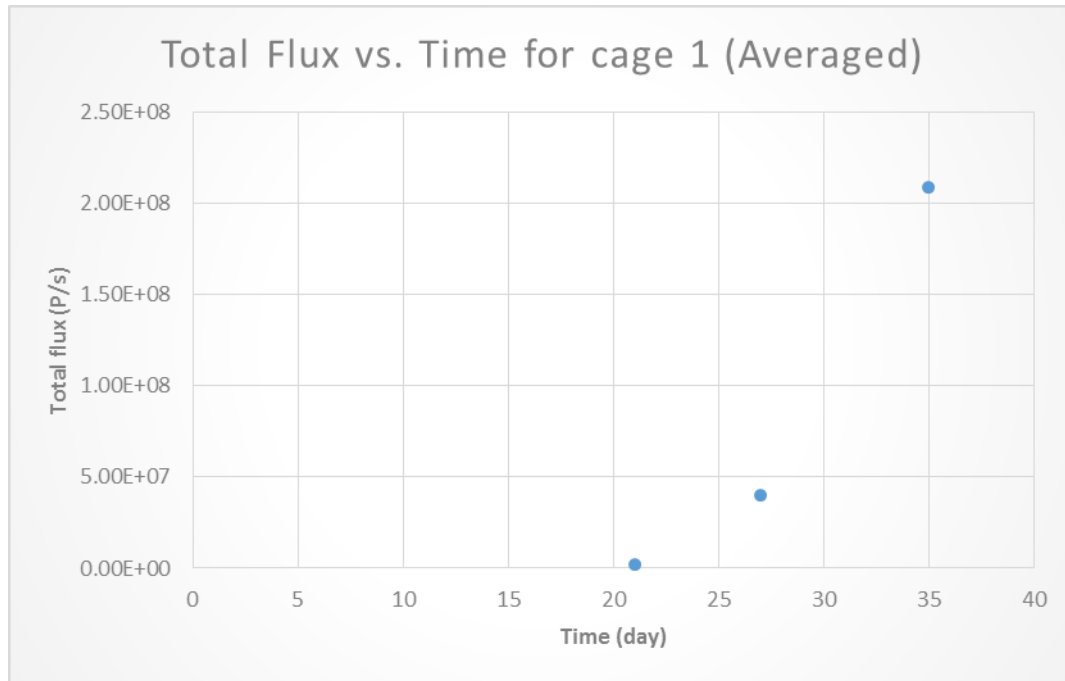
Figure 3.6 Total Flux vs. Time from Cage One (Averaged)

The averaged data also shows that the photon emission and therefore the tumor volume increased at an increasing rate of growth.

For the experiment conducted by Dr. Debinski et.al knowing the change in photon emission flux was sufficient. However, for this research the goal was to model the tumor volume change and therefore the photon emission data were converted to approximate the volume of the tumor in units of mm^3. The photon emission measures luminescence which is an indirect and not completely precise measure of tumor dimensions. However, because these tumors are intracranial,

they cannot be measured directly. In order to quantitate the signal, each cell line must be imaged

to determine the number of photons/cell. This measurement must be done for each cell line because

the signal is dependent on the amount of the genes transfected and expressed. This is done by

preparing a serial dilution of the cell line. Luciferin is added and the cells are imaged to generate

a standard curve. Unfortunately, this has not been done for the cell line used in this experiment.

Photon flux from the tumor is proportional to the number of live cells expressing luciferase

so bioluminescence correlates directly with tumor size. [43]

$$P = K \times N,$$

where P is the photon emission per second, N is the number of cells and K is a constant.

It was assumed in this research that the volume of the tumor is the sum of the volumes of each cell

in the tumor body. Therefore it can be concluded that photon emission is also proportional to the

volume of the tumor.

$$P = K' \times V,$$

where P is the photon emission per second, V is the tumor volume and K' is a constant. k' was

approximately found to be $1.44 \times 10^6 \ \frac{Photon/_s}{mm^3}$ using the Signal vs. Tumor Volume plot shown in

figure 3.7.
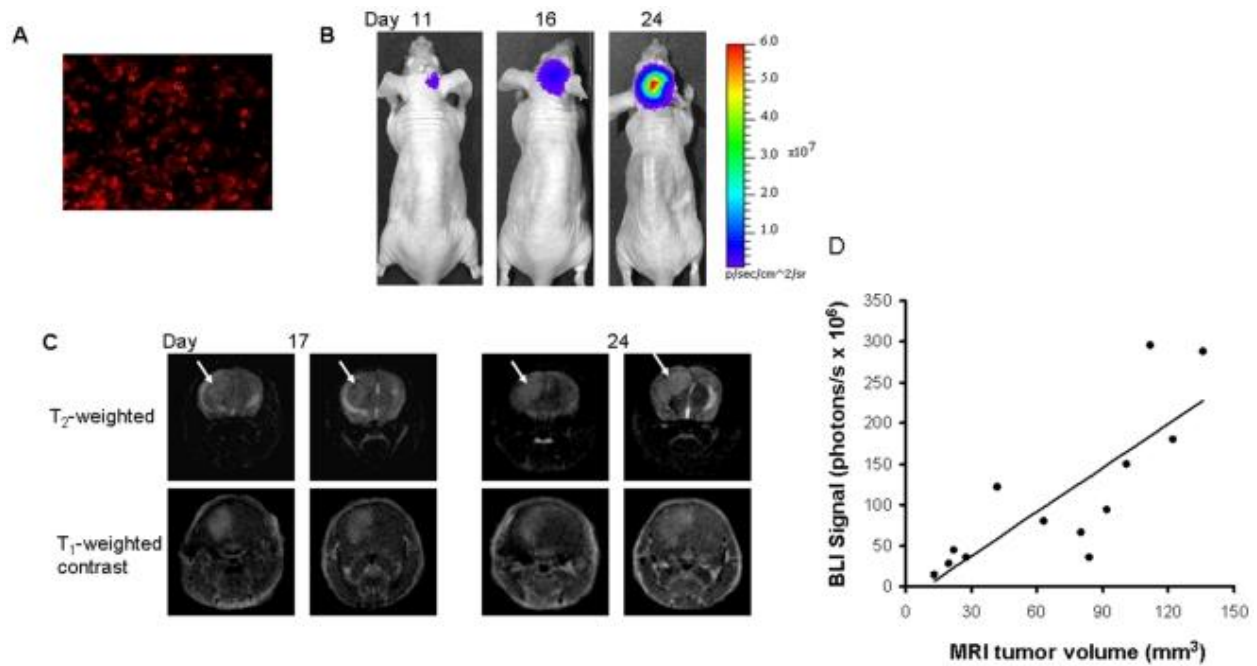
Figure 3.7 Monitoring of intracranial growth of glioblastoma in a mouse [44]

The averaged total flux data from table 3.5 was converted to volume in mm^3 using K' and represented in table 3.6 and figure 3.8.

Table 3.6 In-Vivo Mice Experiment Averaged Data from Cage One in mm^3

Averaged volume [mm^3]	Date and Time	Group	Time Point
1.633846154	3/26/2011 9:09	Cage 1	Week 4
27.69230769	4/1/2011 18:54	Cage 1	Week 5
144.6923077	4/9/2011 16:04	Cage 1	Week 6
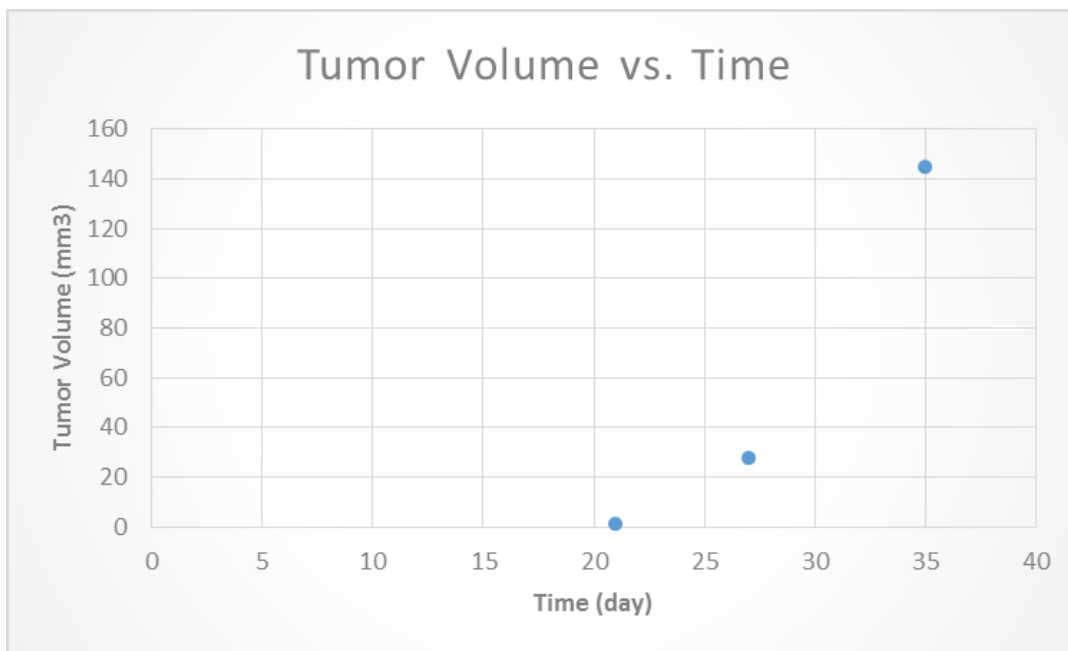
Figure 3.8 Volume vs. Time from Cage One (Averaged)

By the same procedure explained for the data in cage 1, the data for cage 2 were averaged

and changed to the tumor volume. The data from cage 2 is presented in tables 3.7.

Table 3.7 In-Vivo Mice Experiment Data from Cage Two

ROI	Total Flux [p/s]	Date and Time	Time Point
ROI 1	4.84E+05	3/26/2011 9:14	Week 4
ROI 2	1.34E+06	3/26/2011 9:14	Week 4
ROI 3	1.96E+06	3/26/2011 9:14	Week 4
ROI 4	2.36E+06	3/26/2011 9:14	Week 4
ROI 5	4.43E+06	3/26/2011 9:14	Week 4
ROI 1	1.13E+06	4/1/2011 18:58	Week 5
ROI 2	2.26E+06	4/1/2011 18:58	Week 5
ROI 3	2.73E+06	4/1/2011 18:58	Week 5
ROI 4	1.46E+06	4/1/2011 18:58	Week 5
ROI 5	2.33E+06	4/1/2011 18:58	Week 5
ROI 1	1.03E+05	4/9/2011 16:08	Week 6
ROI 2	2.14E+05	4/9/2011 16:08	Week 6
ROI 3	1.20E+07	4/9/2011 16:08	Week 6
ROI 4	1.40E+06	4/9/2011 16:08	Week 6

Table 3.8 and figure 3.9 show the data from mouse 1 in cage 2:

Table 3.8 In-Vivo Mice Experiment Data from Cage Two Mouse One

ROI	Total Flux [p/s]	Date and Time	Group	Time Point
ROI 1	4.84E+05	3/26/2011 9:14	Cage 2	Week 4
ROI 1	1.13E+06	4/1/2011 18:58	Cage 2	Week 5
ROI 1	1.03E+05	4/9/2011 16:08	Cage 2	Week 6
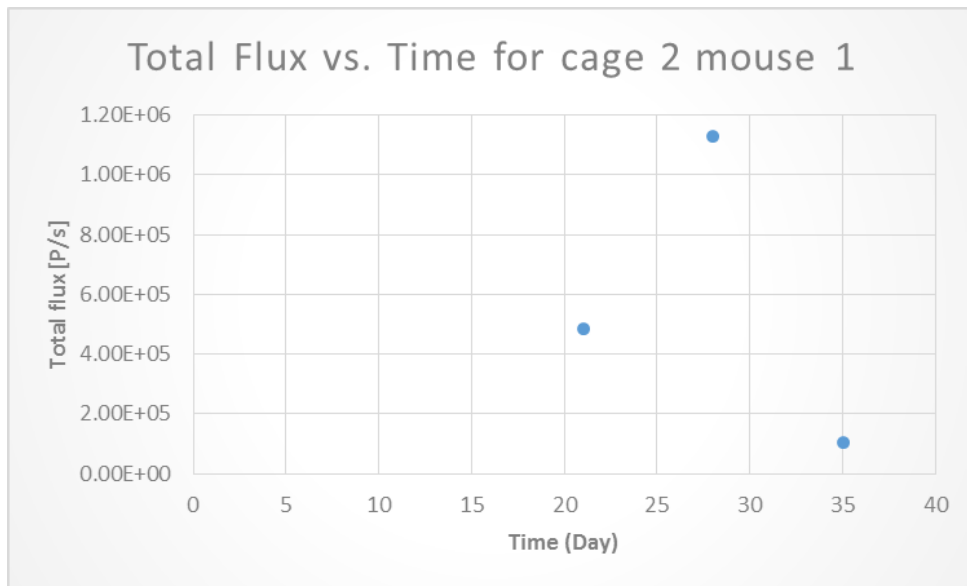
Figure 3.9 Total Flux vs. Time from Cage Two Mouse One

As seen in table 3.8 and figure 3.9, the photon emission decreased which shows that the chemotherapy drug caused the volume of the tumor to decrease.

Table 3.9 and figure 3.10 show the data from mouse 2 in cage 2:

23

Table 3.9 In-vivo Mice Experiment Data from Cage Two Mouse Two

ROI	Total Flux [p/s]	Date and Time	Group	Time Point
ROI 2	1.34E+06	3/26/2011 9:14	Cage 2	Week 4
ROI 2	2.26E+06	4/1/2011 18:58	Cage 2	Week 5
ROI 2	2.14E+05	4/9/2011 16:08	Cage 2	Week 6
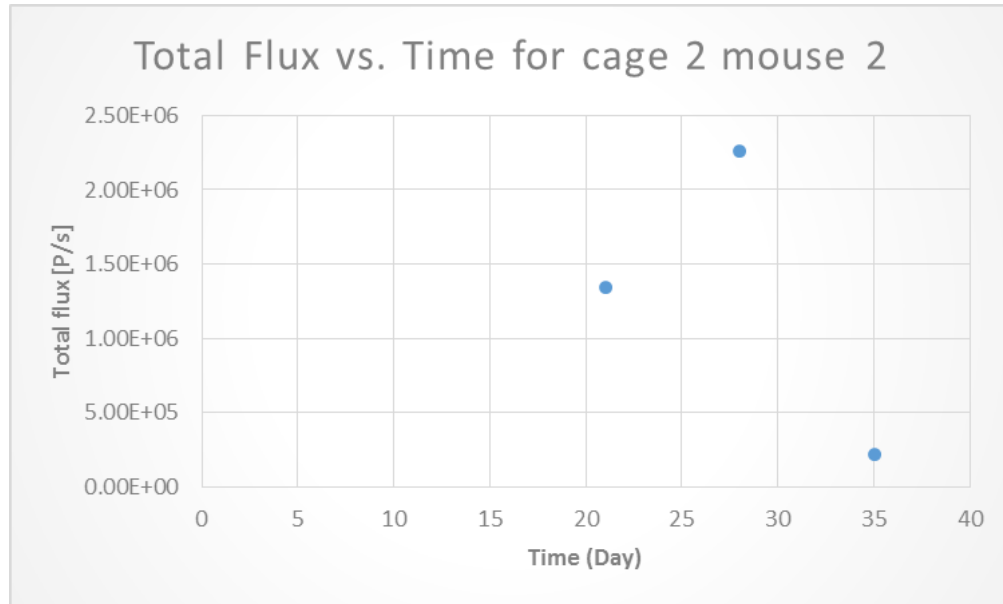
Figure 3.10 Total Flux vs. Time from Cage Two Mouse Two

As seen in table 3.9 and figure 3.10, the photon emission decreased which shows that the chemotherapy drug caused the volume of the tumor to decrease. This is similar to the results from IVIS imaging of mouse 1 from cage 2.

Table 3.10 and figure 3.11 show the data from mouse 3 in cage 2:

Table 3.10 In-Vivo Mice Experiment Data from Cage Two Mouse Three

ROI	Total Flux [p/s]	Date and Time	Group	Time Point
ROI 3	1.96E+06	3/26/2011 9:14	Cage 2	Week 4
ROI 3	2.73E+06	4/1/2011 18:58	Cage 2	Week 5
ROI 3	1.20E+07	4/9/2011 16:08	Cage 2	Week 6
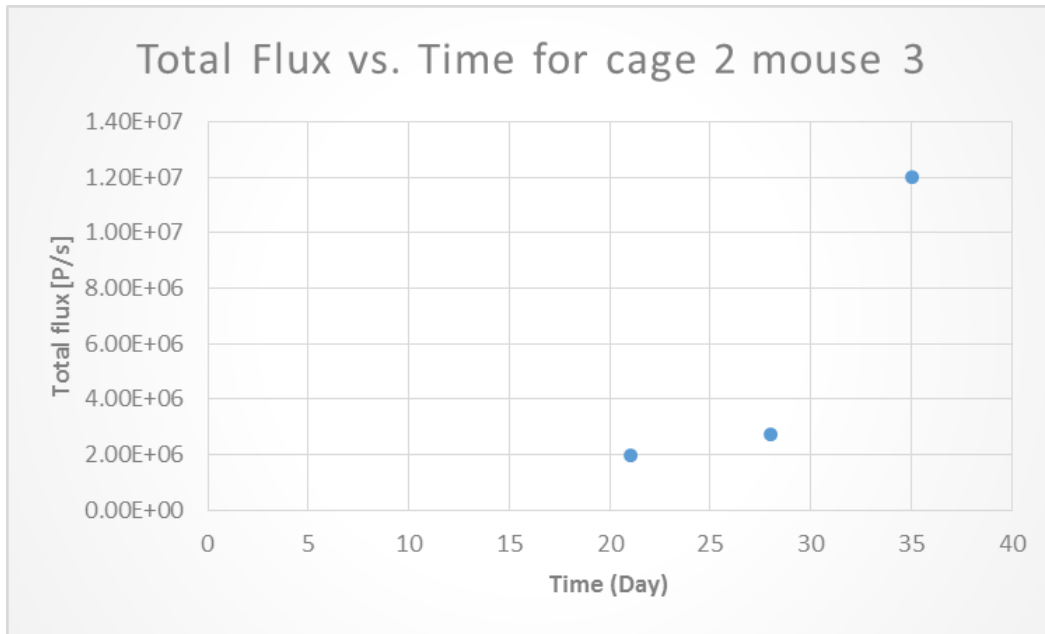
Figure 3.11 Total Flux vs. Time from Cage Two Mouse Three

It can be seen from Figure 3.11 that results from mouse 3 does not show the effect of chemotherapy as expected. The photon emission and therefore the volume of the tumor increase despite the chemotherapy. Because of that the data from mouse 3 was not use further in this research.

Table 3.11 and figure 3.12 show the data from mouse 4 in cage 2:

Table 3.11 In-Vivo Mice Experiment Data from Cage Two Mouse Four

ROI	Total Flux [p/s]	Date and Time	Group	Time Point
ROI 4	2.36E+06	3/26/2011 9:14	Cage 2	Week 4
ROI 4	1.46E+06	4/1/2011 18:58	Cage 2	Week 5
ROI 4	1.40E+06	4/9/2011 16:08	Cage 2	Week 6
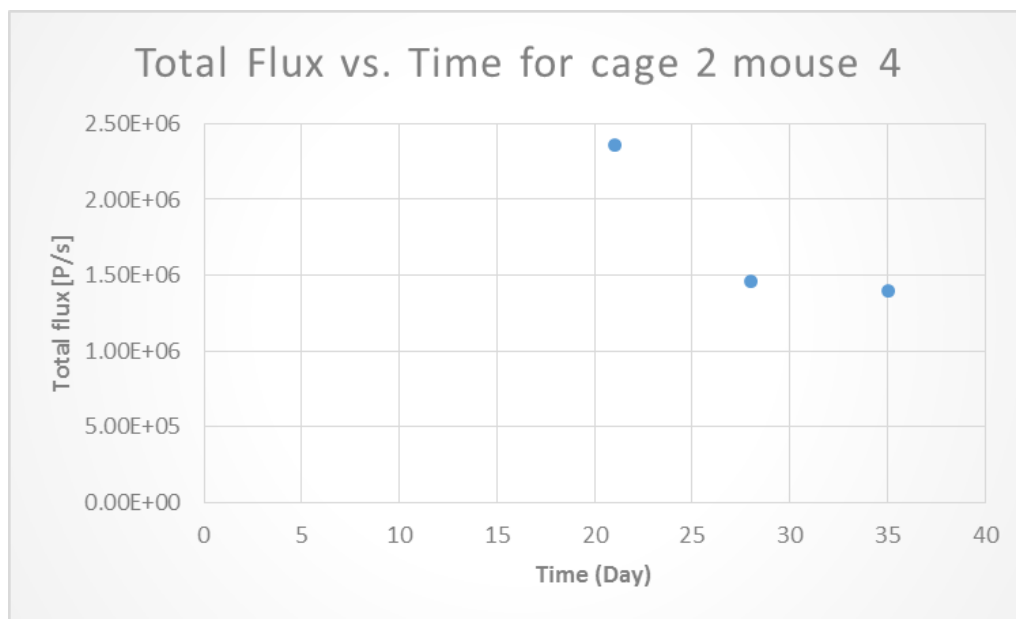
Figure 3.12 Total Flux vs. Time from Cage Two Mouse Four

Table 3.11 and Figure 3.12 show that because of the chemotherapy, photon emission decreased which shows that the volume of the tumor decreased. The decrease that can be seen in mouse 4 is different than mice 1 and 2 as the decrease can be seen between days 21 and 27 and it slowed after day 27. Mouse 5 was sacrificed in this experiment and there is no data available for it for week 6 IVIS imaging. For modeling the effect of chemotherapy the photon emission data was averaged to be later use in the data fitting process.Table 4.6 and figure 4.5 show the data from cage 1 mice 1, 2, 4 and 4 averaged:

Table 3.12 In-Vivo Mice Experiment Averaged Data from Cage Two

ROI	Total Flux [p/s]	Date and Time	Group	Time Point
ROI 4	9.13E+05	3/26/2011 9:14	Cage 2	Week 4
ROI 4	1.7E+06	4/1/2011 18:58	Cage 2	Week 5
ROI 4	1.58E+05	4/9/2011 16:08	Cage 2	Week 6
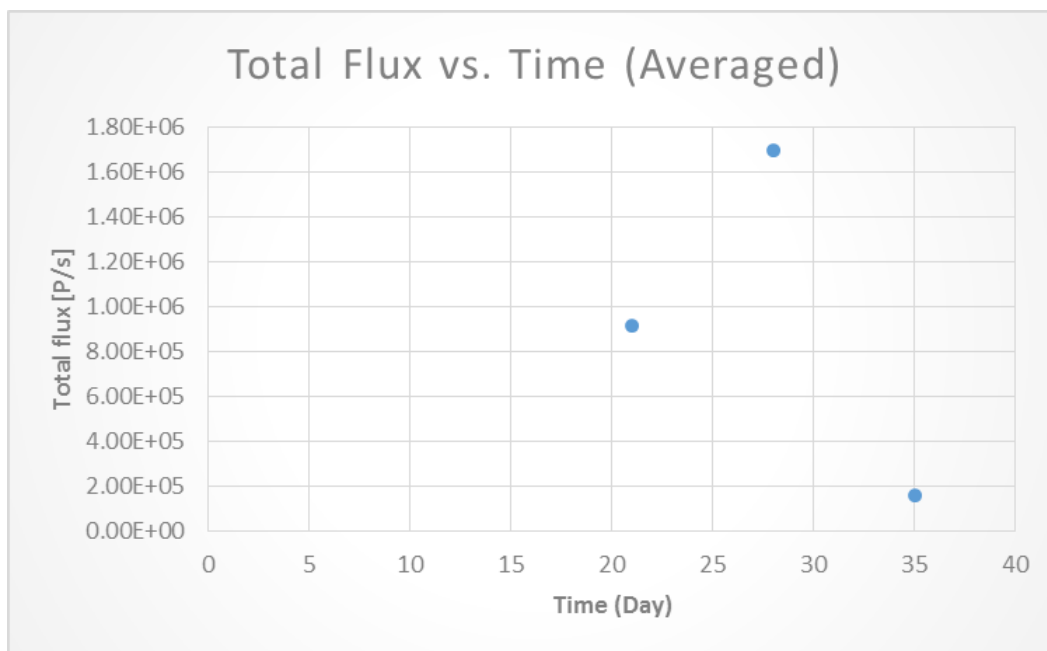
Figure 3.13 Total Flux vs. Time from Cage Two (Averaged)

The photon emission data were changed to approximate volume of the tumor with the same method explained. The averaged emission data from table 3.12 changed to volume in mm^3 and represented in table 3.13 and figure 3.14.

Table 3.13 In-Vivo Mice Experiment Averaged Data from Cage Two in mm^3

Tumor Volume [mm^3]	Date and Time	Group	Time Point
6.032	3/26/2011 9:14	Cage 2	Week 4
11.232	4/1/2011 18:58	Cage 2	Week 5
1.044	4/9/2011 16:08	Cage 2	Week 6
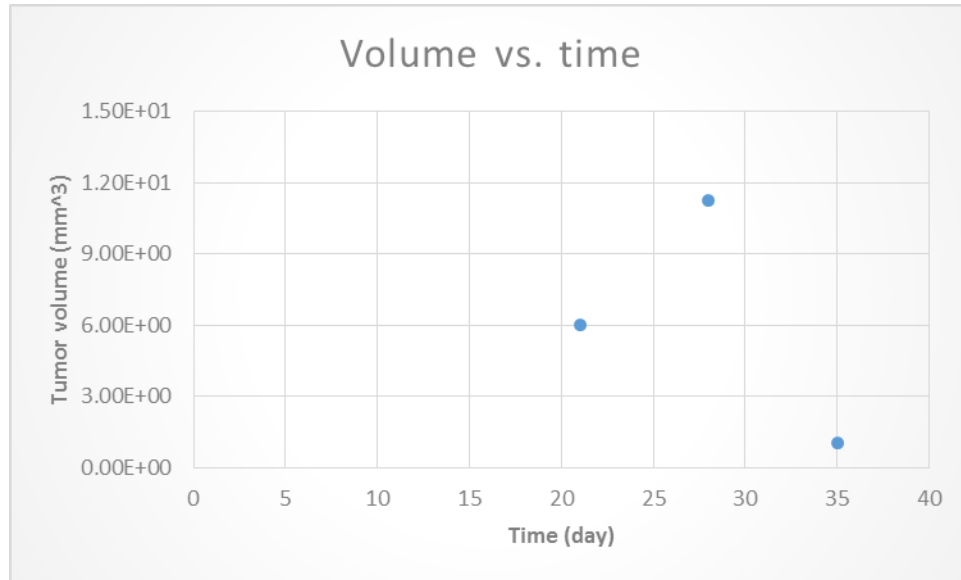
Figure 3.14 Volume vs. Time from Cage Two (Averaged)

3.3 Modeling the natural growth of glioblastomas

There are many mathematical models describing growth. In this part five most common models that were used in this research are presented in form of ordinary differential equations. The behavior of each model is explained in more detail. The behavior of each mathematical model is controlled by the model parameters. Model parameters were found for each type of model that minimized the squared error between the modal and the data found experimentally.

Optimized model parameters were found by the lsqcurvefit function within MATLAB's optimization toolbox. The function lsqcurvit, solves nonlinear curve-fitting (data fitting) problems using least-squares method. The function starts at an initial value x_0 and finds coefficients x to best fit the nonlinear function to the data. More information about this function can be found in MATLAB help.[45]

As an example, the code for the modeling and optimization of the exponential model is presented here. The first part of the code shows the experimental data and this experimental data

stored as vectors. Data in vector format will be used later for fitting the models to the

experimental data and plotting the optimized models.

```matlab
% Experimental data
initial_volume=0.26; %mm3
tumor_volume_21=1.633846154; %mm3 averaged from cage 1
tumor_volume_27=27.69230769; %mm3 averaged from cage 1
tumor_volume_35=144.6923077; %mm3 averaged from cage 1
% Variables
xdata=[1 21 27 35];
ydata=[0.26 1.633846154 27.69230769 144.6923077];
t=linspace(1,35);
```

In the next part of the code, the model was defined and lsqcurvefit function was used to

optimize the model and fit the model to experimental data. For using lsqcurvefit function, an

initial value should be given to the function for unknown parameters. This initial value should be

reasonable or the optimization method will not work properly. The initial values for the unknown

parameters was found from different sources which are presented in table B1 in Appendix B.

Then the optimized model and experimental data were plotted.

```matlab
% Exponential Model

a0=0.1;
N1=@(x,xdata)(initial_volume*(exp(x*xdata)));
[x,resnorm] = lsqcurvefit(N1,a0,xdata,ydata)
N1_Opt=@(t)(initial_volume*(exp(0.1803*t)));
figure(1)
plot(t,N1_Opt(t));
hold on
plot(1,initial_volume,'*',21,tumor_volume_21,'*',…
…27,tumor_volume_27,'*',35,tumor_volume_35,'*');
title('Tumor Volume Growth (Exponential model)')
ylabel('Tumor volume (mm3)')
xlabel('Time (days)')
legend('Exponential','experimental data');
hold on
```

The complete code for all the models can be found in Appendix C.

After the models were optimized and the characteristic parameters obtained for each

model, the models were compared to determine which model fit the experimental data best. For

that, the residual norm given by the lsqcurvefit function in MATLAB was used. The model with

the least residual norm, has the least error and is the best model for the experimental data.

In the following sections five classical models are used to model the tumor growth

behavior. Optimized model parameters are found for each using the methods described above.

3.3.1 Exponential

The ordinary differential equation for this model is,

$$\frac{dV(t)}{dt} = aV(t), \text{ (3.1)}$$

where V is the tumor volume, t is time and a is the growth rate.

Equation 3.1 can be solved as follows:

$$\frac{dV(t)}{dt} = aV(t),$$

Separating the time and volume variables yields,

$$\frac{dV(t)}{V(t)} = adt,$$

Integrating from both side,

$$\int \frac{dV(t)}{V(t)} = \int adt,$$

$$\ln V(t) = at + c,$$

Taking exponential from both sides gives,

$$V(t) = e^{at+c},$$

$$V(t) = e^{at}e^{c},$$

To find what e^c is, t is put equal to zero then,

$$V(0) = e^{c},$$

Substituting $V(0)$ instead of e^c,

$$V(t) = V(0)e^{at}, \text{ (3.2)}$$

In the exponential growth model the tumor growth goes to infinity as time goes to infinity.

$$\lim_{t\to\infty} V(0)e^{at} = \infty$$

Defining the exponential function in MATLAB and using lsqcurvefit function from optimization toolbox the unknown parameter was found.

$$\frac{dV(t)}{dt} = aV(t),$$

$$V(t) = V(0)e^{at},$$

where $V(t)$ is the tumor volume and $V(0) = 0.26 \ mm^3$. In the exponential model, a is the proliferation rate of the tumor cells and it was found to be a=0.1803 day^{-1}.

Then the model and the experimental data were plotted as seen in figure 3.15.
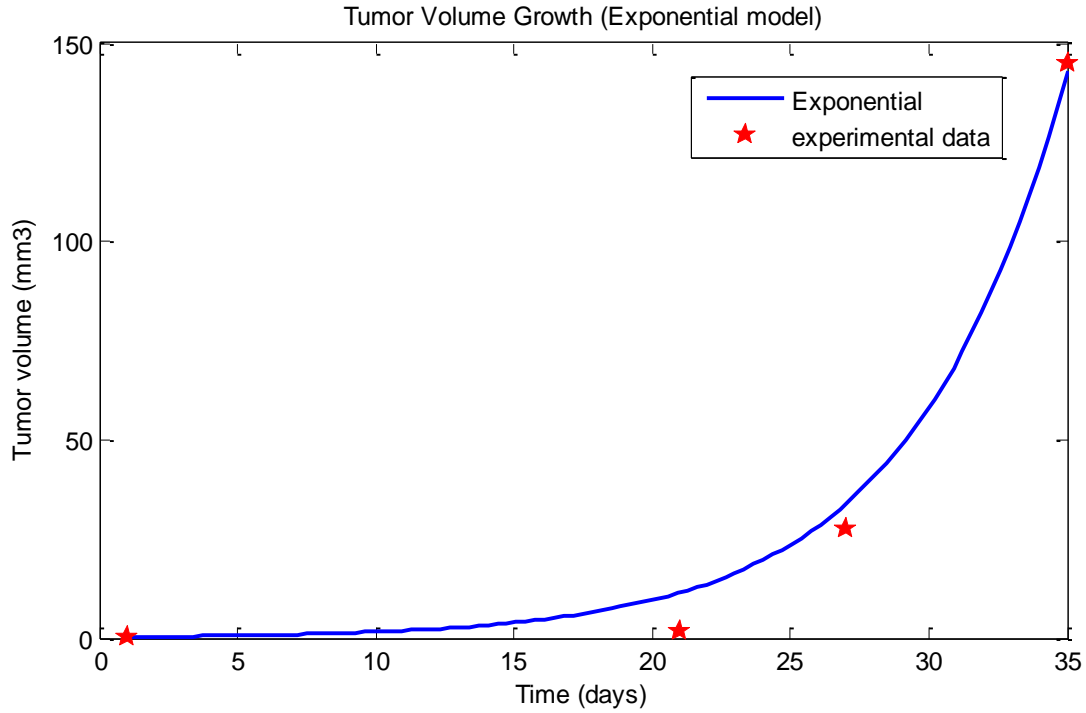
Figure 3.15 Tumor Volume vs. Time (Exponential Model)

3.3.2 Logistic

The ordinary differential equation for this model is,

$$\frac{dV(t)}{dt} = aV(t)\left(1 - \frac{V(t)}{K}\right), \text{(3.3)}$$

where, V is the tumor volume, t is time, a is the proliferation rate and K is the carrying capacity.

Equation 3.3 can be solved as follow:

$$\frac{dV(t)}{dt} = aV(t)(1 - \frac{V(t)}{K}),$$

Separating the time and volume variables yields,

$$\frac{dV(t)}{V(t)(1 - \frac{V(t)}{K})} = adt,$$

Rewriting 1 in the denominator as $\frac{K}{K}$,

$$\frac{dV(t)}{V(t)(\frac{K-V(t)}{K})} = adt,$$

Integrating from both sides yields to,

$$\int \frac{KdV(t)}{V(t)(K-V(t))} = \int adt,$$

$$\int [\frac{1}{V(t)} + \frac{1}{K-V(t)}]dV(t) = \int adt,$$

$$\int \frac{1}{V(t)} dV(t) + \int \frac{1}{K-V(t)} dV(t) = \int adt,$$

$$lnV(t) - ln(K - V(t)) = at + c,$$

$$ln\frac{V(t)}{K-V(t)} = at + c,$$

Taking exponential from both sides gives,

$$\frac{V(t)}{K-V(t)} = e^{at+c},$$

$$\frac{V(t)}{K-V(t)} = e^{at}e^{c},$$

Rearranging the equation to isolate $V(t)$ and finding C by putting t=0, yield to,

$$V(t) = (K - V(t))e^{at}C, \ [C = \frac{V(0)}{K-V(0)}]$$

$$V(t) = \frac{KV(0)}{V(0)+(K-V(0))e^{-at}}, (3.4)$$

The logistic growth model is more realistic in the latter stages of growth than the exponential growth model because it takes in to accounts the limitations. Logistic model has a sigmoid shape, i.e. an increasing curve with one inflection point that asymptotically converges to a maximal volume, the carrying capacity. [7] In the logistic the tumor volume goes to the carrying capacity as time goes to infinity.

$$\lim_{t \to \infty} \frac{KV(0)}{V(0)+(K-V(0))e^{-at}} = K$$

The logistic function was modeled in MATLAB. The optimized model parameters were found using *lsqcurvefit* function in the optimization toolbox. K which is the carrying capacity was set to be $420 \ mm^3$ which is the volume of a 7 week old nude mouse brain.

$$\frac{dV(t)}{dt} = aV(t)\left(1 - \frac{V(t)}{K}\right),$$

$$V(t) = \frac{KV(0)}{V(0)+(K-V(0))e^{-at}},$$

where $V(t)$ is the tumor volume and $V(0) = 0.26 \ mm^3$. In the logistic model a is the proliferation rate of the tumor cells and it was found to be a=0.1911 day^{-1}.

The model and the experimental data were plotted (Figure 3.16).
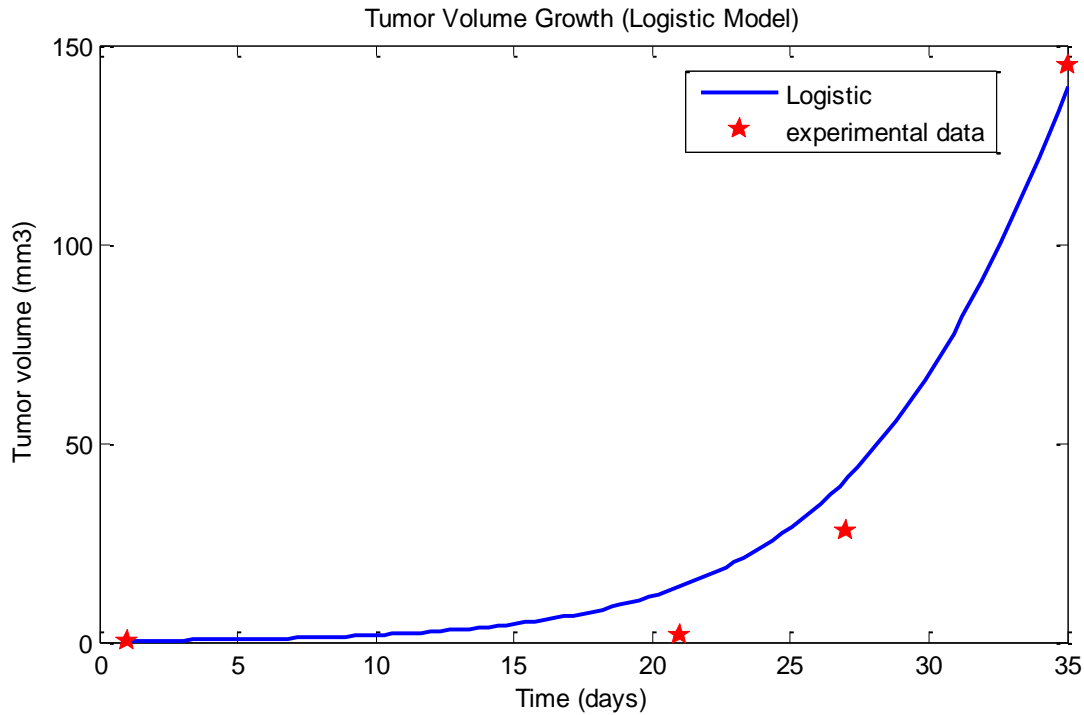
Figure 3.16 Tumor Volume vs. Time (Logistic Model)

3.3.3 Generalized logistic or Richards

The ordinary differential equation for this model is,

$$\frac{dV(t)}{dt} = aV(t)\left(1 - \left(\frac{V(t)}{K}\right)^{\nu}\right), \text{(3.5)}$$

where, V is the tumor volume, t is time, a is the growth rate, K is the tumor volume maximum possible size considering the environment limits also known as the carrying capacity and ν affects how smooth the curve is approaching the carrying capacity.

Equation 3.5 can be solved as follow:

$$\frac{dV(t)}{dt} = aV(t)\left(1 - \left(\frac{V(t)}{K}\right)^{\nu}\right),$$

Separating the time and volume variables yields,

35

$$\frac{dV(t)}{V(t)(1-(\frac{V(t)}{K})^v)} = adt,$$

Rewriting 1 in the denominator as $\frac{K^v}{K^v}$,

$$\frac{dV(t)}{V(t)(\frac{K^v-V(t)}{K^v})} = adt,$$

Integrating from both sides yields,

$$\int \frac{K^v dV(t)}{V(t)(K^v-V(t))} = \int adt,$$

$$\int [\frac{1}{V(t)} + \frac{1}{K^v-V(t)}]dV(t) = \int adt,$$

$$\int \frac{1}{V(t)} dV(t) + \int \frac{1}{K^v-V(t)} dV(t) = \int adt,$$

$$lnV(t) - ln(K^v - V(t)) = at + c,$$

$$ln\frac{V(t)}{K^v-V(t)} = at + c,$$

Taking exponential from both sides gives,

$$\frac{V(t)}{K^v-V(t)} = e^{at+c},$$

$$\frac{V(t)}{K^v-V(t)} = e^{at}e^c,$$

Rearranging the equation to isolate $V(t)$ and finding C by putting t=0, yield to,

$$V(t) = (K^v - V(t))e^{at}C, \quad [C = \frac{V(0)}{K^v-V(0)}]$$

$$V(t) = \frac{KV(0)}{(V(0)^\nu + (K^\nu - V(0)^\nu)e^{-a\nu t})^{\frac{1}{\nu}}} , (3.6)$$

In the logistic growth, the tumor volume goes to the carrying capacity as time goes to infinity.

$$\lim_{t \to \infty} \frac{KV(0)}{(V(0)^\nu + (K^\nu - V(0)^\nu)e^{-a\nu t})^{\frac{1}{\nu}}} = K$$

Defining the generalized logistic function in MATLAB and using lsqcurvefit function within the optimization toolbox the unknown parameters were found. K which is the carrying capacity was set to be $420 \ mm^3$ which is the volume of a 7 week old nude mouse brain.

$$\frac{dV(t)}{dt} = aV(t)(1 - (\frac{V(t)}{K})^\nu),$$

$$V(t) = \frac{KV(0)}{(V(0)^\nu + (K^\nu - V(0)^\nu)e^{-a\nu t})^{\frac{1}{\nu}}} ,$$

where $V(t)$ is the tumor volume and $V(0) = 0.26 \ mm^3$. In the generalized logistic model, a is the initial proliferation rate of the tumor cells and it was found to be a=0.18 day⁻¹. Also ν was found to be 18. The model and the experimental data were plotted (Figure 3.17).

Figure 3.17 Tumor Volume vs. Time (Generalized Logistic Model)

3.3.4 Gompertz

The ordinary differential equation for this model is,

$$\frac{dV(t)}{dt} = ae^{-\beta t}V(t), \ (3.7)$$

where, V is the tumor volume, t is time, a is the initial proliferation rate and β is the rate exponential decay of this proliferation rate.

Equation 3.7 can be solved as follow:

$$\frac{dV(t)}{dt} = ae^{-\beta t}V(t),$$

Separating the time and volume variables yields,

$$\frac{dV(t)}{V(t)} = ae^{-\beta t}dt,$$

38

Integrating from both sides,

$$\int \frac{dV(t)}{V(t)} = \int ae^{-\beta t} dt,$$

$$\ln V(t) = -\frac{a}{\beta} e^{-\beta t} + c,$$

Taking exponential from both sides,

$$V(t) = e^{-\frac{a}{\beta} e^{-\beta t} + c},$$

$$V(t) = e^{-\frac{a}{\beta} e^{-\beta t}} e^c,$$

Rearranging the equation to isolate $V(t)$ and finding C by putting t=0, yield to,

$$V(t) = e^{-\frac{a}{\beta} e^{-\beta t}} C, \ [C = V(0)e^{\frac{a}{\beta}}]$$

$$V(t) = V(0)e^{\frac{a}{\beta}(1 - e^{-\beta t})},$$

Gompertz model shows exponential decay of the relative growth rate. Asymptotically the volume of the tumor converges to the carrying capacity which is,

$$\lim_{t \to \infty} V(0)e^{\frac{a}{\beta}(1 - e^{-\beta t})} = V(0)e^{\frac{a}{\beta}}.$$

Defining the Gompertz function in MATLAB and using lsqcurvefit function from optimization toolbox the unknown parameters were found.

$$\frac{dV(t)}{dt} = ae^{-\beta t}V(t),$$

$$V(t) = V(0)e^{\frac{a}{\beta}(1 - e^{-\beta t})},$$

Where $V(t)$ is the tumor volume and $V(0) = 0.26 \; mm^3$. The unknown parameters in this model are a, and β. In the Gompertz model a which is the initial proliferation rate of the tumor cells, was found to be and to be 0.183 day^{-1} and the rate exponential decay of this proliferation rate β was found to be 0.001 day^{-1}. Then the model and the experimental data were plotted in figure 3.18.
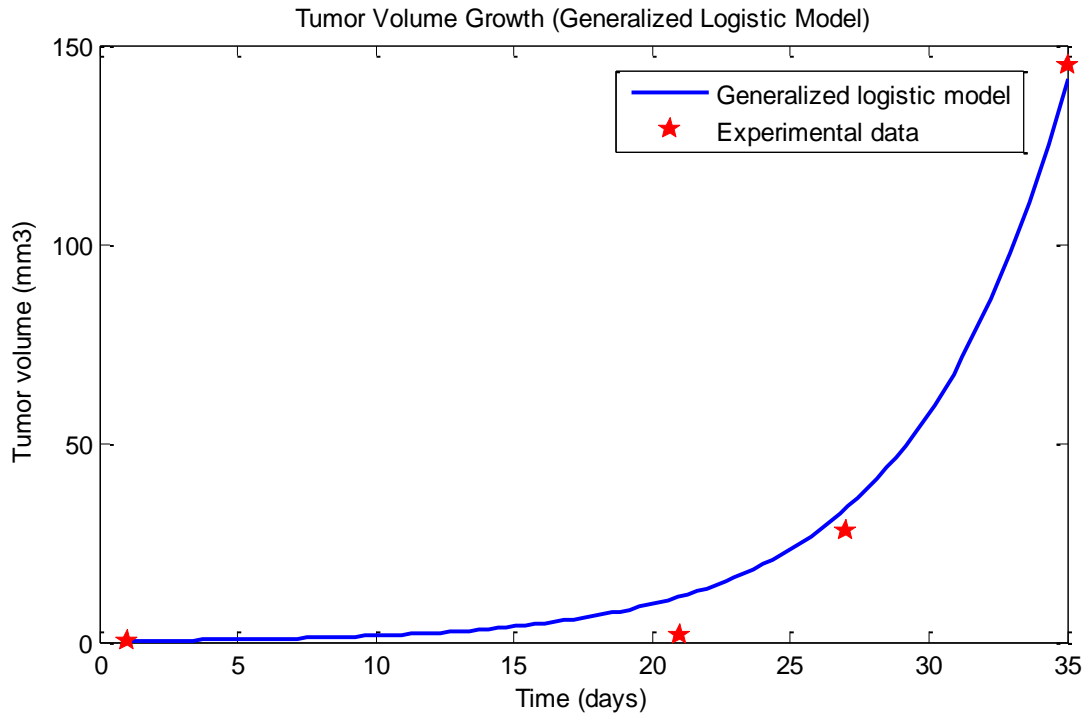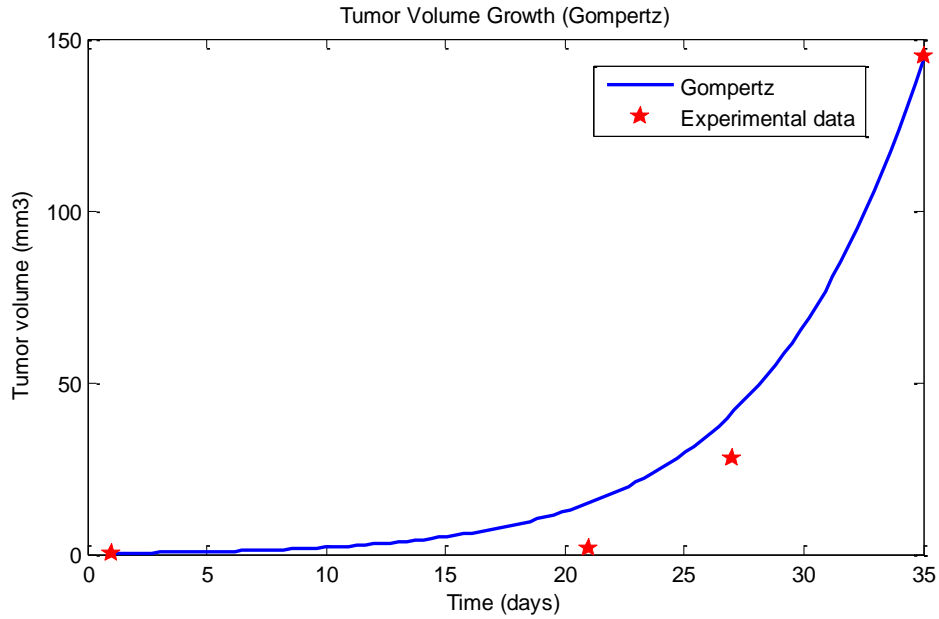

Figure 3.18 Tumor Volume vs. Time (Gompertz Model)

3.3.5 Von Bertalanffy

The ordinary differential equation for this model is,

$$\frac{dV(t)}{dt} = aV(t)^{\gamma} - bV(t), \text{ (3.8)}$$

Equation 3.9 was solved using Wolfram Mathematical by the command below:

$$V(t) = \left(\frac{a}{b} + (V(0)^{1-\gamma} - \frac{a}{b})e^{-b(1-\gamma)t}\right)^{\frac{1}{1-\gamma}}, \text{ (3.10)}$$

Defining the Von Bertalanffy function in MATLAB and using lsqcurvefit function from optimization toolbox the unknown parameters were found.

$$\frac{dV(t)}{dt} = aV(t)^\gamma - bV(t),$$

$$V(t) = \left(\frac{a}{b} + (V(0)^{1-\gamma} - \frac{a}{b})e^{-b(1-\gamma)t}\right)^{\frac{1}{1-\gamma}},$$

Where $V(t)$ is the tumor volume and $V(0) = 0.26 \ mm^3$. In the Von Bertalanffy model showing the volume of tumor growth, b and γ has the same amount as found before, whereas a should have a unit change. a was found to be $0.7057 \ mm^{3(1-\gamma)}. day^{-1}$. Then the model and the experimental data were plotted in figure 3.19.
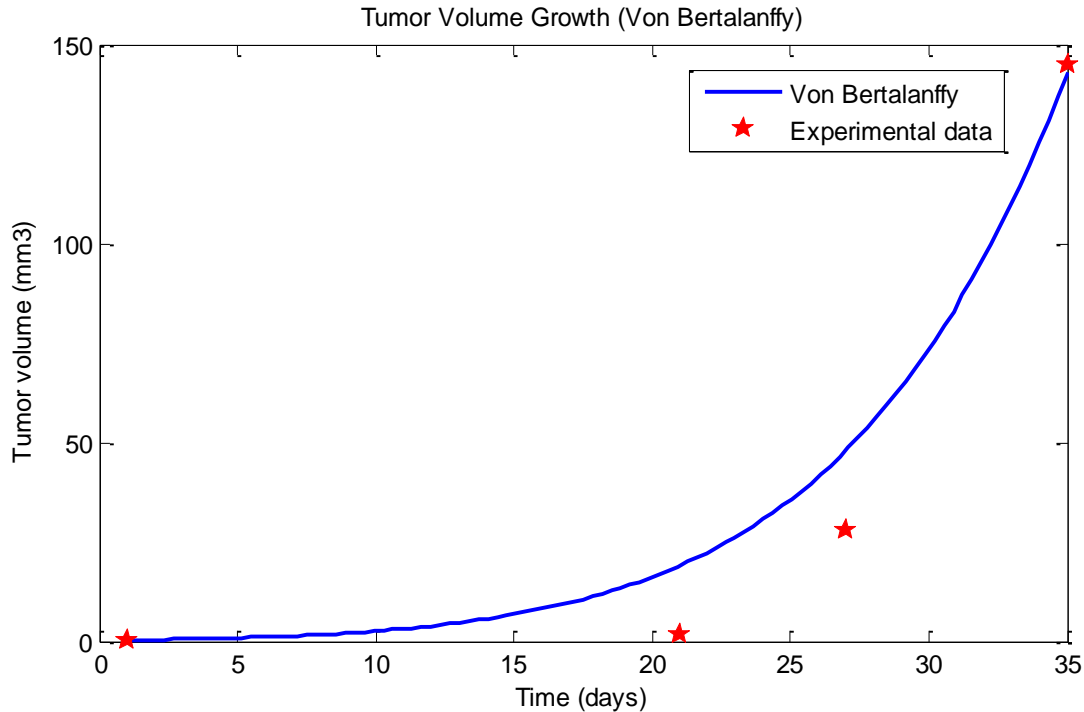
Figure 3.19 Tumor Volume vs. Time (Von Bertalanffy)

3.4 Models comparison

Examination of the plots shown in Figures 3.9 through 3.13 reveal that all five classical models can fit the experimental data points reasonably well after the optimization. In addition, their shapes are very similar for the early stages of tumor growth. The goal of this part of the research besides optimizing each model and finding the unknown parameters, was to find the model that fit the data best among these five models. This could lead to a better understanding the tumor growth behavior. The optimization function lsqcurvefit also calculates the residual norm. Residual norm is a good parameter to evaluate the goodness of fit for each models. The residual norm for each function is shown in table 3.14. Also the plots of all the optimized models can be seen in figure 3.20.

Table 3.14 Models Characteristic Parameters and the Residual Norms

Mathematical Model	Unknown Parameter	Unit	Parameter Values	Residual norm $[mm^6]$
Exponential	a	$[day^{-1}]$	0.179	137
Logistic	a	$[day^{-1}]$	0.1911	351
	K	$[mm^3]$	420	
Generalized Logistic	a	$[day^{-1}]$	0.18	137
	K	$[mm^3]$	420	
	υ	-	18	
Gompertz	α	$[day^{-1}]$	0.25	43
	β	$[day^{-1}]$	0.02	
Von Bertalanffy	a	$[mm^{3(1-\gamma)}.day^{-1}]$	0.25	45
	b	$[day^{-1}]$	0.024	
	γ	-	0.9	
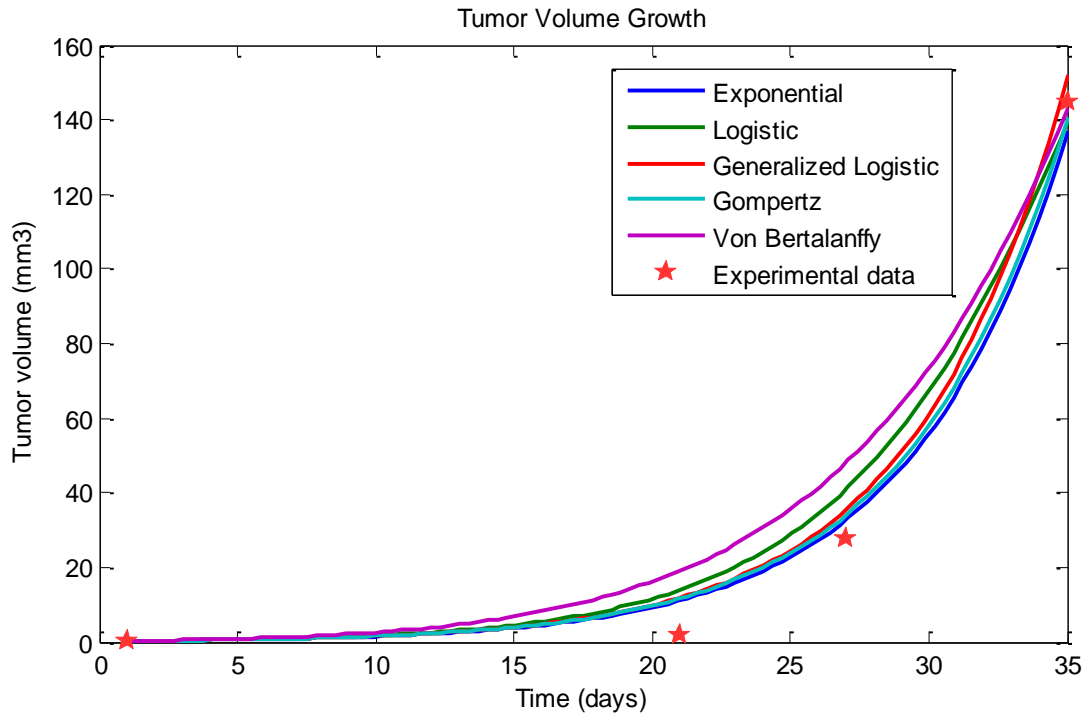
Figure 3.20 Tumor Volume vs. Time (Models Comparison)

Looking at the residual norms in table 3.14 reveals the Gompertz model to have the least residual norm. Another factor to identify the best model is the number of unknown parameters in the model. A simple model with less parameters is a better model. We can see that the exponential model has one unknown parameters, logistic and Gompertz model have two and Generalized logistic and Von Bertalanffy have three. Based on the residual norms and also the number of unknown parameters it can be seen that Gompertz model is the best fitting among the five classical models.

CHAPTER 4: MODELING THE EFFECT OF CHEMOTHERAPY

4.1 Developing the chemotherapy model

First the Gompertz model which was optimized was plotted on the same graph with the experimental data from cage 2.
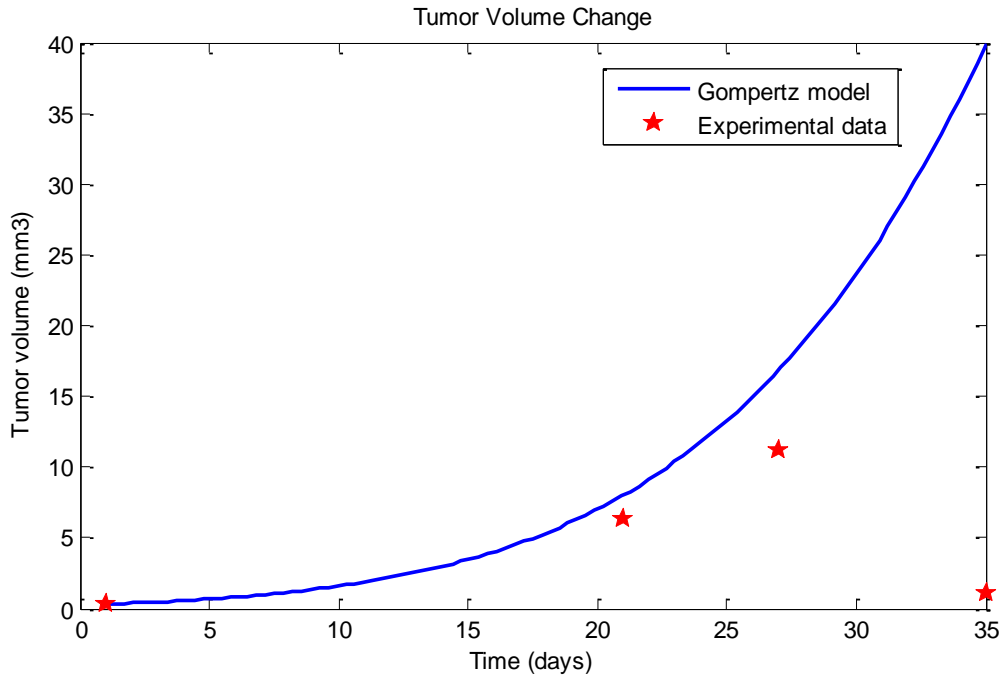
Figure 4.1 Gompertz Model and the Experimental Data from Cage Two

As seen in figure 4.1, Gompertz model fits the data before the chemotherapy phase begins quite well and then chemotherapy effects the growth of the tumor.

After chemotherapy the growth of the tumor becomes slower, then the volume begins to decrease. This is an expected and desired outcome of chemotherapy and it indicates that F10 may be a promising chemotherapy drug for glioblastomas as also mentioned in [7]. Recall from section 2.6 that F10 is the thymidylate synthase (TS) inhibitory metabolite of 5-fluorouracil (5-FU). [27]

This effects the excessive proliferation of tumor cells and also kills some of the tumor cells. For modeling the effect of chemotherapy these factors must be considered.

Chemotherapy treatment occurred over a 7 days period but our model for chemotherapy has an instant start and it effect remains the same afterwards. This is called an on-off effect. Therefore the model for representing the data from cage two is a piecewise equation:

$$
\begin{cases}
\text{Gompertz model,} & \text{Before chemotherapy} \\
\text{Gompertz model + the effect of chemotherapy,} & \text{After chemotherapy}
\end{cases}
$$

Our model evaluated three different start times for adding the effect of chemotherapy, the first day of the chemotherapy (day 21), the last day of the chemotherapy (day 27) and the day in the middle of the chemotherapy process (day 25). This day is defined as the transition time in the model, t_T.

Using the first day of chemotherapy models a fast dynamic system response to the drug. The effect of chemotherapy begins instantly (in the model) and is maintained by continued chemotherapy over the week of treatment and beyond. Using the last day of chemotherapy models a slow dynamic system response to the drug. The effect of chemotherapy take time before an observable effect occurs. Using the midpoint of treatment models a moderate dynamical system response. Understanding which model fits best will provide insight into the dynamic response of the system which may be useful in developing optimized treatment protocols.

4.2 Developed chemotherapy model

Before the chemotherapy begins the model is the Gompertz model found in the previous chapter. After the chemotherapy starts, again the base is the Gompertz model with an added part showing the effect of chemotherapy. It was assumed that a percentage of the tumor cells died every day because of the chemotherapy and leave the tumor body immediately. The compartment model of it can be seen in figure 4.2.
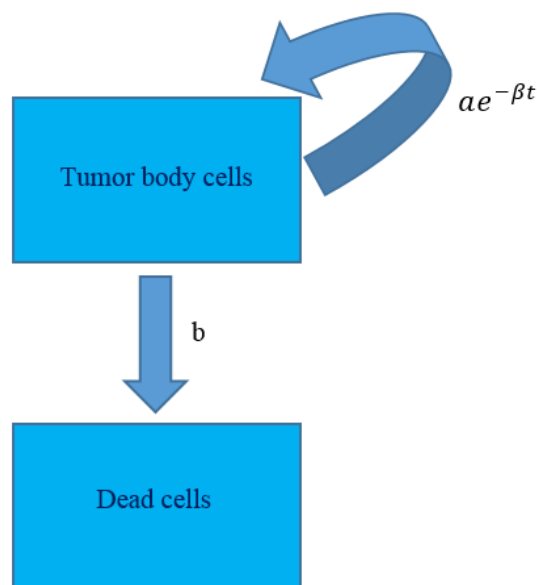
Figure 4.2 Chemotherapy Effect Compartment Model

The piecewise ordinary differential equation of it, is as follow:

$$
\begin{cases}
\dfrac{dV(t)}{dt} = ae^{-\beta t}V(t), & \text{Before } t_T \\[2ex]
\dfrac{dV(t)}{dt} = ae^{-\beta t}V(t) - bV(t), & \text{After } t_T
\end{cases}
$$

46

The solution of the ordinary differential equation of the model, is as follow:

$$V(t) = V(0)e^{\frac{a}{\beta}(1-e^{-\beta t})}, \qquad\qquad\qquad \text{Before day } t_T$$

$$V(t) = V(0)e^{\frac{a}{\beta}(1-e^{-\beta t})-b(t-t_{ch})}, \qquad\qquad\qquad \text{After day } t_T$$

This model was fit to the data using lsqcurvefit function in MATLAB and plotted for each value of t_T.(Figures 4.3 - 4.5)
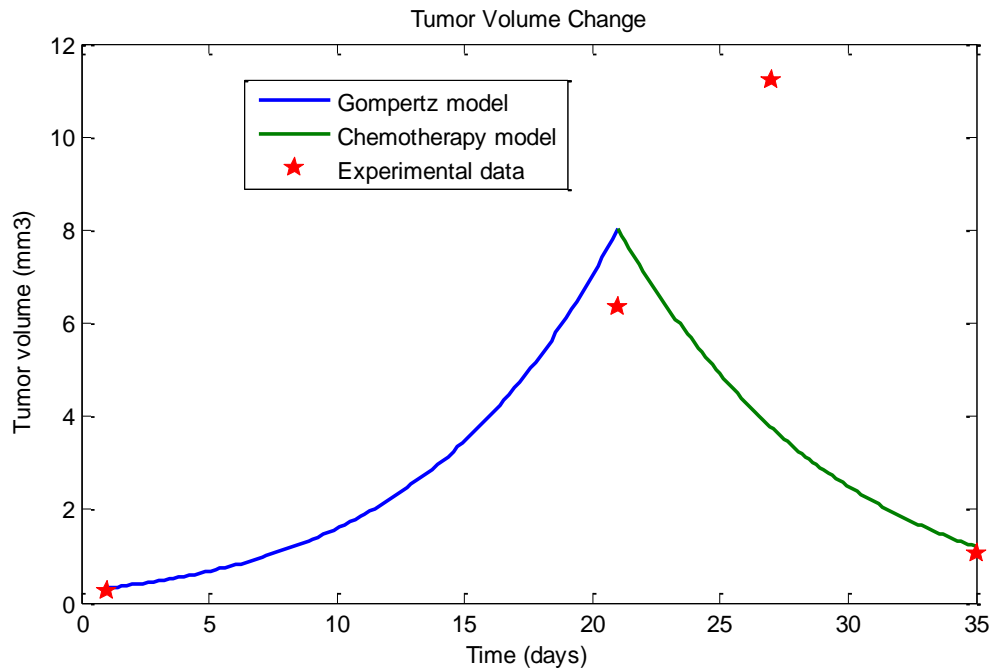
Figure 4.3 Fast Dynamic Response: t_T = day 21
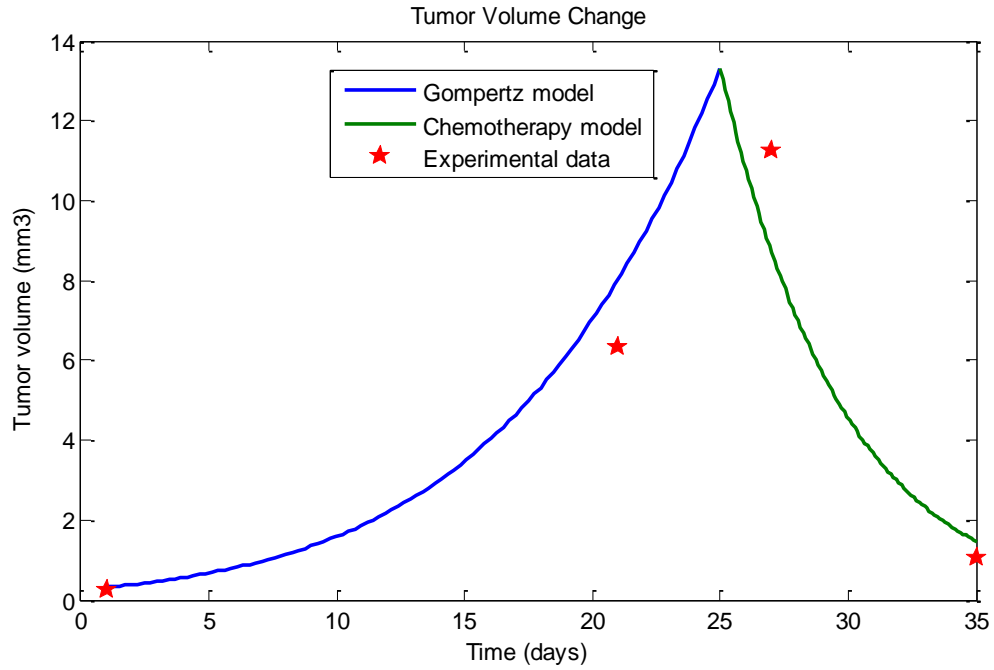
Figure 4.4 Moderate Dynamic Response: t_T = day 25
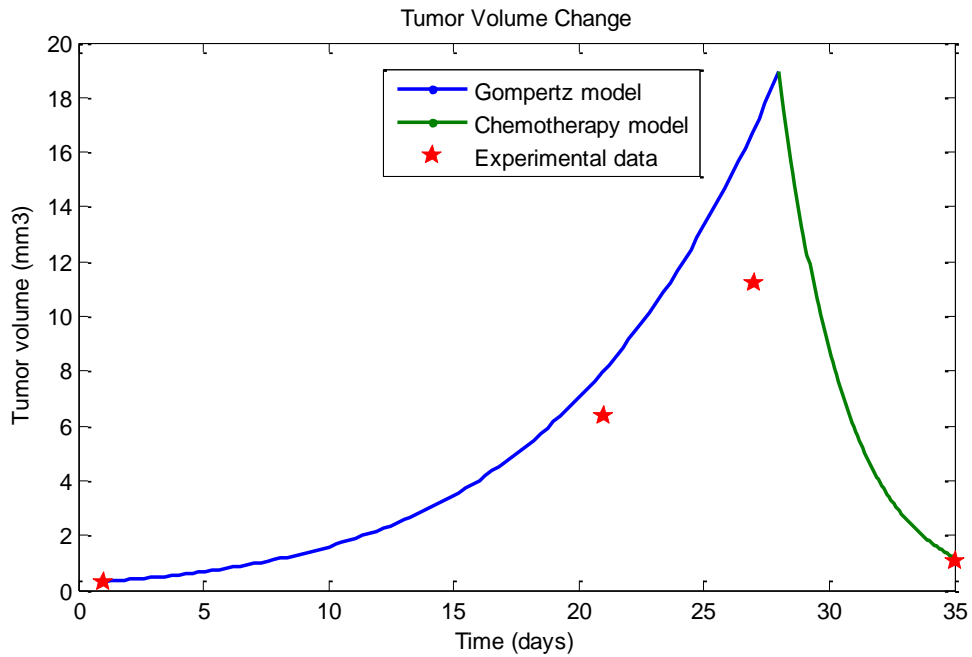
Figure 4.5 Slow Dynamic Response: tT = day 28

As seen in figures 4.3 through 4.5, in the first developed chemotherapy model when the chemotherapy starts, a dramatic change in the slope can be seen, meaning that the speed of tumor volume change, suddenly decreased by a great amount. From data fitting, b was found to be 0.3 day^{-1}. The complete code for this part can be found in Appendix D.

The other point that can be seen from these figures is that the time assumed for the beginning of the effect of chemotherapy, is an important factor in who could the model fits. Therefore all three of them were plotted in one figure for comparison in figure 13 to find the best fit.
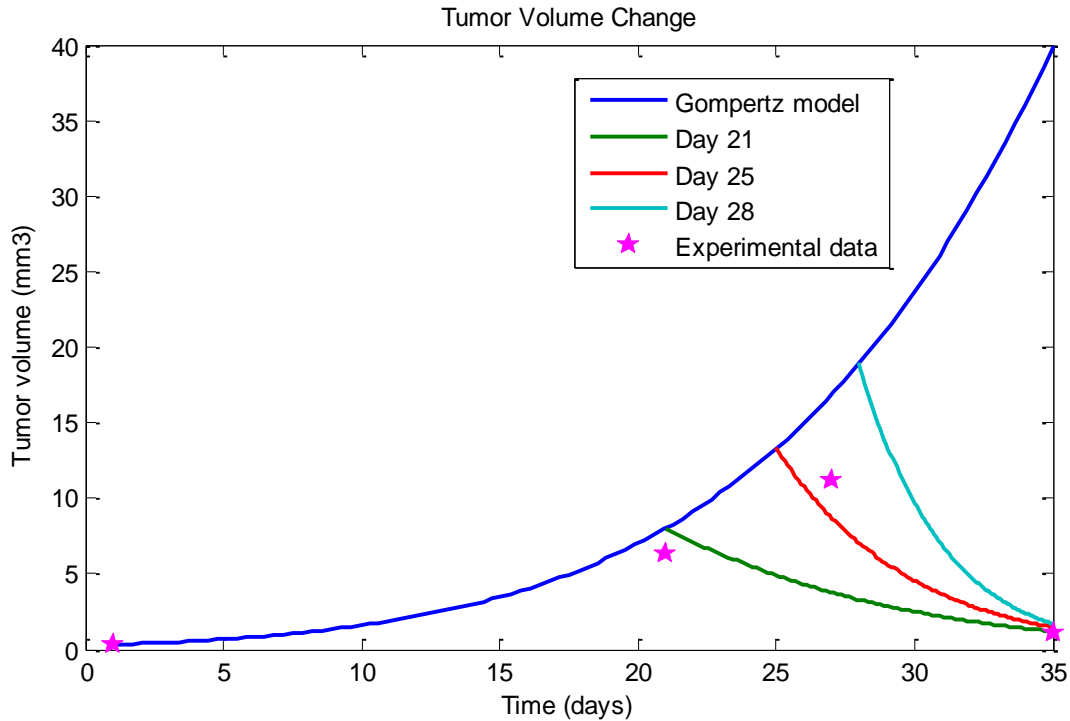
Figure 4.6 Gompertz Model, Chemotherapy Model and the Experimental Data from Cage Two

Based on the result from the comparison of the 3 different chemotherapy start days, it can be found that considering day 25 results in a better fit. This suggests that in a 7 day chemotherapy treatment, the effect starts to show itself more in the middle of the treatment period rather than in

the beginning or the end of it. This result can be used in the treatment procedure and period decisions.

4.3 Model sensitivity analysis

In mathematical modeling it is important to know the sensitivity of the model to each of its parameters. In this part the sensitivity of the model to each of the model parameters is found. In the Gompertz model, showing only the natural growth of the tumor before chemotherapy the sensitivity of the function to α and β are found. The MATLAB code of the sensitivity analysis can be found in appendix E.

$$V(t) = V(0)e^{\frac{a}{\beta}(1-e^{-\beta t})},$$

$$S\left(V(t), \alpha\right) = \frac{\partial V(t)}{\partial \alpha} \times \frac{\alpha}{V(t)} = \frac{1}{\beta}(1 - e^{-\beta t}) \, V(0)e^{\frac{a}{\beta}(1-e^{-\beta t})} \times \frac{\alpha}{V(t)}$$

$$S\left(V(t), \beta\right) = \frac{\partial V(t)}{\partial \beta} \times \frac{\beta}{V(t)} = V(0)(-\frac{a}{\beta^2}(1 - e^{-\beta t}) + \frac{a}{\beta}(te^{-\beta t}))e^{\frac{a}{\beta}(1-e^{-\beta t})} \times \frac{\beta}{V(t)}$$
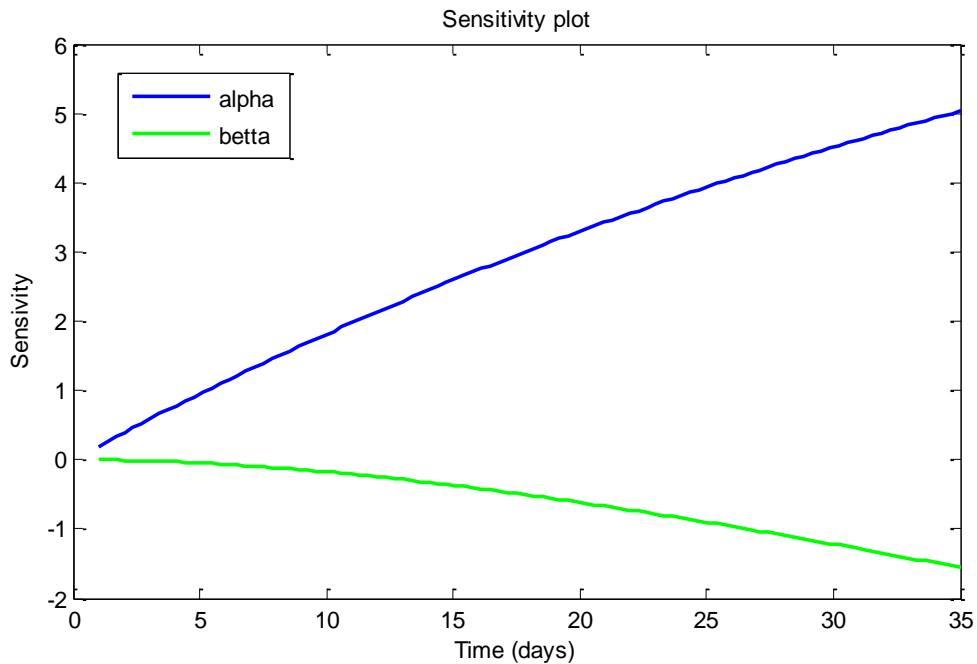
Figure 4.7 Gompertz Natural Growth Model Sensitivity Plot

In the modified Gompertz model, showing the effect of chemotherapy on the tumor growth, the sensitivity of the function to α, β and b are found.

50

$$V(t) = V(0)e^{\frac{a}{\beta}(1-e^{-\beta t})-bt},$$

$$S\left(V(t),\alpha\right) = \frac{\partial V(t)}{\partial \alpha} \times \frac{\alpha}{V(t)} = \left(\frac{1}{\beta}(1-e^{-\beta t}) - bt\right)V(0)e^{\frac{a}{\beta}(1-e^{-\beta t})-bt} \times \frac{\alpha}{V(t)}$$

$$S\left(V(t),\beta\right) = \frac{\partial V(t)}{\partial \beta} \times \frac{\beta}{V(t)} = V(0)\left(-\frac{a}{\beta^2}\left(1-e^{-\beta t}\right) + \frac{a}{\beta}\left(te^{-\beta t}\right)\right)e^{\frac{a}{\beta}(1-e^{-\beta t})-bt} \times \frac{\beta}{V(t)}$$

$$S\left(V(t),b\right) = \frac{\partial V(t)}{\partial b} \times \frac{b}{V(t)} = -V(0) \times t \times e^{\frac{a}{\beta}(1-e^{-\beta t})-bt} \times \frac{b}{V(t)}$$
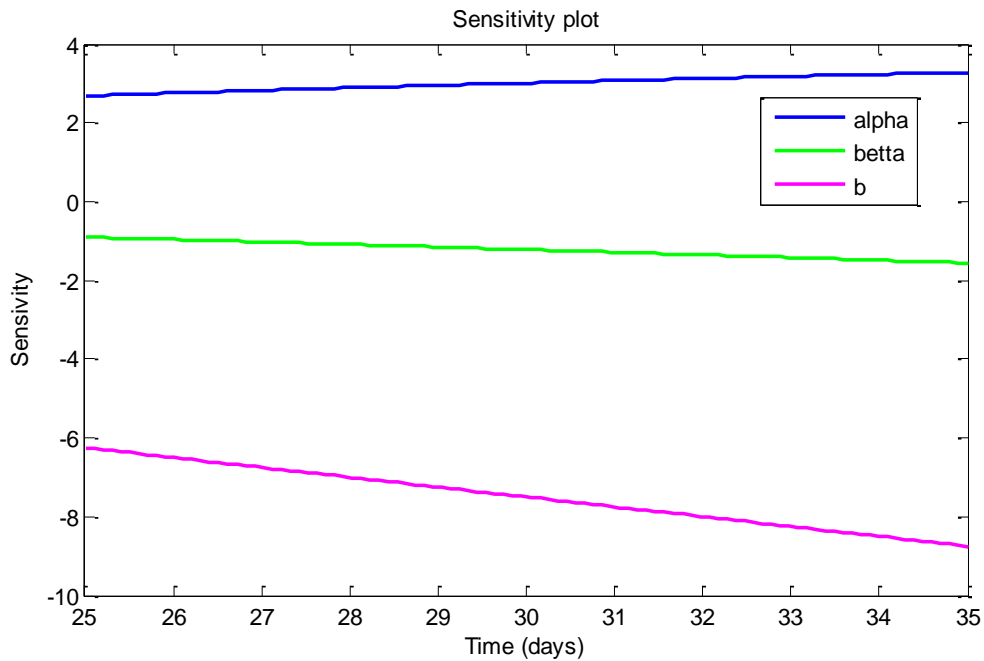
Figure 4.8 Modified Gompertz Chemotherapy Effect Model Sensitivity Plot

CHAPTER 5: CONCLUSION AND FUTURE WORK

5.1 Conclusion

In this research five classical tumor growth mathematical models were used to model the natural growth of glioblastoma. The models evaluated were the exponential, logistic, generalized logistic, Gompertz and Von Bertallanfy models. The characteristic parameters of each of the models were found by fitting the mathematical models to data from an in-vivo experiment on nude mice performed at Wake Forest University School of Medicine. Upon evaluation, the Gompertz model was determined be the best fit having the lowest residual norm.

Next the effect of chemotherapy with F10 on glioblastoma growth was modeled. Gompertz model developed for the natural tumor growth was used and the effect of chemotherapy was added to the model. The combined model was piecewise continuous and changed slope at the transition time, t_T. The model accounted for natural tumor growth until prior to the transition time and modeled tumor behavior under the influence of chemotherapy after the transition time. The results from the chemotherapy model shows that the model fits the data better with the delay time of $t_T = 25$ and therefore it can be said that there is a moderate response time to F10.

These model can be used for developing more understanding on tumor growth behavior. Also using the models, virtual tests can be run to predict the effect of different forms of chemotherapy. By doing this lots of time and money can be saved. Moreover the models can later be used for preliminary testing and treatment options for glioblastomas.

5.2 Future work

In this research the only concentration of chemotherapy evaluated was 80 mg/kg (data from cage 2). The data for higher dosages 120 mg/kg (cage 3) and 160 mg/kg (cage 4) will be modeled

in future studies. These high dosages of chemotherapy drug F10 also resulted in more tumor shrinkage. [7] The concentration of F10 may also be entered as a component in the model to improve the model's precision or extend its ability to predict tumor volume changes for difference concentrations. These models can help to guide future experiments. The data from cages 3 and 4 can be found in Appendix A.

In the current study chemotherapy was consider to be and on-off process. However, in the actual experiment F10 was administered over a period of 7 days. Future models could take this into account. Finally, measuring data at shorter intervals will provide better insight into the characteristic shape of the curves improving the type of model selected and the accuracy of the results.

Also looking at Figures 4.2 through 4.5 from chapter 4 it can be noticed that after chemotherapy the rate of tumor volume change, decreases dramatically. Although the presented model is a good fit to the data, for having a more precise model the dramatic drop can be smoothened.

REFERENCES

[1] Heron M, Hoyert D, Murohy S, Xu J, Kochanek K, Tejada-Vera B (2009) Deaths: final data for 2006. Natl. Vital. Stat. Rep. 57, 1-134.

[2] Aldape K, Colman H, James C (2006) Models of malignant glioma. Drug Discov. Today Dis. Models 3, 191-196.

[3] Tanaka, M. L., Debinski, W., & Puris, I. K. (2008). Hybrid mathematical model of glioma progression, Cell Proliferation, 42, pp. 637-646, doi: 10.1111/j.1365-2184.2009.00631.

[4] Hatzikirou H, Deutsch A, Schaller C, Simon M, Swanson K (2005) Mathematical modeling of glioblastoma tumor development: a review. Math. Models Methods Appl. Sci. 15, 1779-1794.

[5] Holland EC (2000) Glioblastoma multiforme: the terminator. Proc. Natl. Acad. Schi. USA 97, 6242-6244.

[6] Weiss W, Aldape K, eds (2007) Nervous System Cancer Models. Bethesda. MD: National Cancer Institute.

[7] Gmeiner, W. H., Lema-Tome, C., Gibo, D., Jennings-Gee, J., Milligan, C. & Debinski, W. (2013). Selective anti-tumor activity of the novel fluoropyrimidine polymer F10 towards G48a orthotopic GBM tumors, Journal of Neuro-Oncology, Vol. 116, No. 3, pp. 447–45, doi: 10.1007/s.11060-013-1321-1

[8] Cooper, M. D., Tanaka, M. L., & Puri, I. K. (2010). Coupled mathematical model of tumorigenesis and angiogenesis in vascular tumors. Cell Proliferation, 43, pp. 542-552, doi: 10/1111/j.1364-2184.2010.00703.

[9] Komarova NL (2005) Mathematical modeling of tumorigenesis: mission possible. Curr. Opin. Oncol. 17, 39-43.

[10] Dorland's Medical Dictionary for Health Consumers. (2007). Retrieved April 7 2015 from http://medical-dictionary.thefreedictionary.com

[11] Astrocytoma. Retrieved January 10, 2016, from http://www.abta.org/brain-tumor-information/types-of-tumors/astrocytoma.html

[12] Chromosomes Fact Sheet. Retrieved November 8, 2014, from https://www.genome.gov/26524120

[13] What is DNA? Retrieved March 2, 2016, from http://www.yourgenome.org/facts/what-is-dna

[14] What is a gene? Retrieved March 5, 2016, from https://ghr.nlm.nih.gov/handbook/basics/gene

[15] Saunders Comprehensive Veterinary Dictionary, 3 ed. (2007). Retrieved April 7 2015 from http://medical-dictionary.thefreedictionary.com

[16] What-is-cancer A Collection of Related Diseases. Retrieved April 7 2015 from http://www.cancer.gov/about-cancer/what-is-cancer A Collection of Related Diseases

[17] What is cancer? Retrieved December 20, 2014, from http://www.cancercenter.com/what-is-cancer/

[18] Weinberg, R. A. (2007). *The biology of cancer*. New York: Garland Science.

[19] Somatic mutation - Glossary Entry. Retrieved August 3, 2015, from https://ghr.nlm.nih.gov/glossary=somaticmutation

[20] Glioblastoma (GBM). Retrieved May 14, 2015, from http://www.abta.org/brain-tumor-information/types-of-tumors/glioblastoma.html

[21] Krex D, Klink B, Hartmann C, von Deimling A, Pietsch T, Simon M, Sabel M, Steinbach JP, Heese O, Reifenberger G, Weller M, Schackert G. Long-term survival with glioblastoma multiforme. Brain. 2007;130(Pt 10):2596–2606. doi: 10.1093/brain/awm204.

[22] Hulleman E, Helin K. Molecular mechanisms in gliomagenesis. Adv Cancer Res. 2005;94:1–27. doi: 10.1016/S0065-230X(05)94001-3.

[23] Astrocytoma. Retrieved February 4, 2016, from http://www.abta.org/brain-tumor-information/types-of-tumors/astrocytoma.html

[24] What is cancer? A guide for patients and families. Retrieved June 15, 2015, from http://www.cancer.org/cancer/cancerbasics/what-is-cancer

[25] NCI Dictionary of Cancer Terms. Retrieved September 2, 2015, from http://www.cancer.gov/publications/dictionaries/cancer-terms?cdrid=386207

[26] Antimetabolites | Drugs.com. Retrieved October 15, 2015, from http://www.drugs.com/drug-class/antimetabolites.html

[27] Thymidylate synthase inhibitors. Retrieved March 6, 2016, from http://www.pharmacorama.com/en/Sections/DNA-RNA-biosynthesis-6.php

[28] Swanson, K. R., Bridge, C., Murray, J., D., Alvord, E., C. (2003). Virtual and real brain tumors: using mathematical modeling to quantify glioma growth and invasion, Journal of the Neurological Sciences, Volume 216, Issue 1, pp. 1–10, doi:10.1016/j.jns.2003.06.001

[29] Murray, J. D., (2002). Mathematical Biology, 3rd ed, Springer-Verlag, New York, NY

[30] Frieboes HB, Lowengrub JS, Wise S, Zheng X, Macklin P, Bearer EL, Cristini V (2007) Computer simulation of glioma growth and morphology, Neuroimage 37(Suppl. 1), S59-S70.

[31] Mcklin P, Lowengrub J (2007) Nonlinear simulation of the effect of microenvironment on tumor growth. J. Theor. Boil. 245, 677-704.

[32] V.P. Collins, R.K. Loeffler, H. Tivey (1956). Observations on growth rates of human tumors Am. J. Roetgenol. Radium Ther. Nucl. Med., 76, pp. 988–1000

[33] S. Kusama, J.S. Spratt Jr., W.L. Donegan, F.R. Watson, C. (1972). CunninghamThe gross rates of growth of human mammary cancerCancer, 30, pp. 594–599

[34] Shackney, S. E. 1993. Tumor Growth, Cell Cycle Kinetics, and Cancer Treatment. McGraw Hill, New York.

[35] Benzekry S, Lamount C, Beheshti A, Tracz A, Ebos JML, Hlatky K et al. (2014) Classical Mathematical Models for Description and Prediction of Experimental Tumor Growth. PLoS Comput Biol 10(8):e1003800

[36] Brú, A., Albertos, S., Subiza, J. L., García-Asenjo, J. L., & Brú, I. (2003). The Universal Dynamics of Tumor Growth. *Biophysical Journal, 85*(5), 2948-2961. doi:10.1016/s0006-3495(03)74715-8

[37] Vaidya VG, Alexandro FJ (1982) Evaluation of some mathematical models for tumor growth. Int J Biomed Comput 13: 19–36 Available: http://www.ncbi.nlm.nih.gov/pubmed/7061168

[38] Spratt JA, von Fournier D, Spratt JS, Weber EE (1993) Decelerating growth and human breast cancer. Cancer 71: 2013–2019 Available: http://www.ncbi.nlm.nih.gov/pubmed/8443753

[39] Casey AE (1934) The experimental alteration of malignancy with an homologous mammalian tumor material: I. Results with intratesticular inoculation. Am J Cancer 21: 760–775.

[40] Norton L (1988) A Gompertzian model of human breast cancer growth. Cancer Res 48: 7067–7071 Available: http://cancerres.aacrjournals.org/content/48/24_Part_1/7067.short Accessed 9 July 2013.

[41] Xenogen IVIS Imaging System 100 | STTARR. Retrieved May 21, 2015, from http://www.sttarr.ca/core2/equipment/xenogen

[42] Retrieved May 26, 2015, from http://www2.udel.edu/ctcr/sites/udel.edu.ctcr/files/IVIS Lumina Tutorial.pdf

[43] Lim, E., Modi, K. D., & Kim, J. (2009). In vivo Bioluminescent Imaging of Mammary Tumors Using IVIS Spectrum. Journal of Visualized Experiments : JoVE, (26), 1210. Advance online publication. http://doi.org/10.3791/1210

[44] Zhou, H., Luby-Phelps, K., Mickey, B. E., Habib, A. A., Mason, R. P., & Zhao, D. (2009). Dynamic Near-Infrared Optical Imaging of 2-Deoxyglucose Uptake by Intracranial Glioma of Athymic Mice. PLoS ONE, 4(11), e8051. http://doi.org/10.1371/journal.pone.0008051

[45] MATLAB R2013a Help

[46] M., Thiessen, J. D., Kurjewicz, L. M., Germscheid, S. L., Turner, A. J., Zhilkin, P., Martin, M. (2010). Longitudinal Brain Size Measurements in APP/PS1 Transgenic Mice. *MRI Magnetic Resonance Insights,* 19. doi:10.4137/mri.s5885

APPENDIX A: IN-VIVO EXPERIMENT RAW DATA

Tables of raw data from the in-vivo experiment

Table A.1 Raw Data for Cage One (Vehicle Treatment Only)

CAGE 1				
Image Number	ROI	Image Layer	Total Flux [p/s]	Date and Time
CLT20110326090936A	ROI 1	Overlay	8.33E+05	3/26/2011 9:09
CLT20110326090936A	ROI 2	Overlay	4.22E+06	3/26/2011 9:09
CLT20110326090936A	ROI 3	Overlay	1.84E+07	3/26/2011 9:09
CLT20110326090936A	ROI 4	Overlay	1.38E+06	3/26/2011 9:09
CLT20110326090936A	ROI 5	Overlay	3.02E+06	3/26/2011 9:09
CLT20110401185357A	ROI 1	Overlay	6.27E+06	4/1/2011 18:54
CLT20110401185357A	ROI 2	Overlay	7.38E+07	4/1/2011 18:54
CLT20110401185357A	ROI 3	Overlay	1.13E+06	4/1/2011 18:54
CLT20110409160428A	ROI 1	Overlay	2.50E+07	4/9/2011 16:04
CLT20110409160428A	ROI 2	Overlay	3.93E+08	4/9/2011 16:04
CLT20110409160428A	ROI 3	Overlay	6.67E+06	4/9/2011 16:04

Table A.2 Raw Data for Cage Two (Treatment with 80 mg/kg of F10)

CAGE 2				
Image Number	ROI	Image Layer	Total Flux [p/s]	Date and Time
CLT20110326091429A	ROI 1	Overlay	4.84E+05	3/26/2011 9:14
CLT20110326091429A	ROI 2	Overlay	1.34E+06	3/26/2011 9:14
CLT20110326091429A	ROI 3	Overlay	1.96E+06	3/26/2011 9:14
CLT20110326091429A	ROI 4	Overlay	2.36E+06	3/26/2011 9:14
CLT20110326091429A	ROI 5	Overlay	4.43E+06	3/26/2011 9:14
CLT20110401185803A	ROI 1	Overlay	1.13E+06	4/1/2011 18:58
CLT20110401185803A	ROI 2	Overlay	2.26E+06	4/1/2011 18:58
CLT20110401185803A	ROI 3	Overlay	2.73E+06	4/1/2011 18:58
CLT20110401185803A	ROI 4	Overlay	1.46E+06	4/1/2011 18:58
CLT20110401185803A	ROI 5	Overlay	2.33E+06	4/1/2011 18:58
CLT20110409160813A	ROI 1	Overlay	1.03E+05	4/9/2011 16:08
CLT20110409160813A	ROI 2	Overlay	2.14E+05	4/9/2011 16:08
CLT20110409160813A	ROI 3	Overlay	1.20E+07	4/9/2011 16:08
CLT20110409160813A	ROI 4	Overlay	1.40E+06	4/9/2011 16:08

Table A.3 Raw Data for Cage 3 (Treatment with 120 mg/kg of F10)

CAGE 3				
Image Number	ROI	Image Layer	Total Flux [p/s]	Date and Time
CLT20110326092314A	ROI 1	Overlay	7.56E+04	3/26/2011 9:23
CLT20110326092314A	ROI 2	Overlay	7.56E+05	3/26/2011 9:23
CLT20110326092314A	ROI 3	Overlay	7.96E+05	3/26/2011 9:23
CLT20110326092314A	ROI 4	Overlay	1.79E+06	3/26/2011 9:23
CLT20110326092314A	ROI 5	Overlay	3.67E+06	3/26/2011 9:23
CLT20110401190228A	ROI 1	Overlay	7.04E+04	4/1/2011 19:02
CLT20110401190228A	ROI 2	Overlay	4.02E+05	4/1/2011 19:02
CLT20110401190228A	ROI 3	Overlay	6.87E+05	4/1/2011 19:02
CLT20110401190228A	ROI 4	Overlay	1.04E+06	4/1/2011 19:02
CLT20110401190228A	ROI 5	Overlay	1.31E+06	4/1/2011 19:02
CLT20110409161148A	ROI 1	Overlay	3.45E+06	4/9/2011 16:11
CLT20110409161148A	ROI 2	Overlay	1.89E+05	4/9/2011 16:11
CLT20110409161148A	ROI 3	Overlay	1.26E+06	4/9/2011 16:11
CLT20110409161148A	ROI 4	Overlay	1.42E+06	4/9/2011 16:11

Table A.4 Raw Data for Cage 4 (Treatment with 160 mg/kg of F10)

CAGE 4				
Image Number	ROI	Image Layer	Total Flux [p/s]	Date and Time
CLT20110326092755A	ROI 1	Overlay	4.98E+05	3/26/2011 9:28
CLT20110326092755A	ROI 2	Overlay	7.35E+05	3/26/2011 9:28
CLT20110326092755A	ROI 3	Overlay	1.88E+06	3/26/2011 9:28
CLT20110326092755A	ROI 4	Overlay	4.00E+05	3/26/2011 9:28
CLT20110326092755A	ROI 5	Overlay	5.85E+05	3/26/2011 9:28
CLT20110401190612A	ROI 1	Overlay	1.62E+06	4/1/2011 19:06
CLT20110401190612A	ROI 2	Overlay	1.66E+06	4/1/2011 19:06
CLT20110401190612A	ROI 3	Overlay	3.17E+06	4/1/2011 19:06
CLT20110401190612A	ROI 4	Overlay	1.29E+06	4/1/2011 19:06
CLT20110401190612A	ROI 5	Overlay	1.17E+06	4/1/2011 19:06
CLT20110409161526A	ROI 1	Overlay	1.19E+06	4/9/2011 16:15
CLT20110409161526A	ROI 2	Overlay	5.74E+06	4/9/2011 16:15
CLT20110409161526A	ROI 3	Overlay	3.14E+07	4/9/2011 16:15
CLT20110409161526A	ROI 4	Overlay	1.25E+06	4/9/2011 16:15

APPENDIX B: TUMOR GROWTH MODEL PARAMETERS

Table B.1 Human Glioblastoma parameter values

Parameter	Values	Units	Source
Cell Radius	0.005	mm	8
Proliferation rate	2.75	1/day	8
Apoptosis rate	0.32	1/day	3

Table B.2 Lung cancer parameter values [35]

Mathematical Model	Unknown Parameter	Unit	Parameter Values
Exponential	a	[day^{-1}]	0.257
Logistic	a	[day^{-1}]	0.502
	K	[mm^3]	1297
Generalized	a	[day^{-1}]	2555
Logistic	K	[mm^3]	4378
	υ	-	0.00014
Gompertz	α	[day^{-1}]	0.743
	β	[day^{-1}]	0.0792
Von Bertalanffy	a	[mm$^{3(1-\gamma)}$.day^{-1}]	7.72
	b	[day^{-1}]	6.75
	γ	-	0.947

APPENDIX C: MATLAB CODE FOR THE NATURAL GROWTH

MATLAB Code for Mathematical modeling of Glioblastoma volume growth

```matlab
% MathematicalModelingofGlioblastoma
% NudeMiceIn-vivoModedlWithoutChemotherapy

clc;
close all;
format long

% Experimental data

initial_volume=0.26; %mm3
tumor_volume_21=1.633846154; %mm3 averaged from cage 1
tumor_volume_27=27.69230769; %mm3 averaged from cage 1
tumor_volume_35=144.6923077; %mm3 averaged from cage 1

% Variables

xdata=[1 21 27 35];
ydata=[0.26 1.633846154 27.69230769 144.6923077];
t=linspace(1,35);

% Exponential Model

a0=0.1;
N1=@(x,xdata)(initial_volume*(exp(x*xdata)));
[x,resnorm] = lsqcurvefit(N1,a0,xdata,ydata)
N1_Opt=@(t)(initial_volume*(exp(0.179*t)));
figure(1)
plot(t,N1_Opt(t));
hold on
plot(1,initial_volume,'*',21,tumor_volume_21,'*',27,tumor_volume_27,'*',35,tu
mor_volume_35,'*');
title('Tumor Volume Growth (Exponential model)')
ylabel('Tumor volume (mm3)')
xlabel('Time (days)')
legend('Exponential','experimental data');
hold on


%Logistic Model

a0=0.3;
N2=@(x,xdata)((initial_volume*420)./(initial_volume+(420-
initial_volume)*exp(-x(1)*xdata)));
[x,resnom] = lsqcurvefit(N2,a0,xdata,ydata)
N2_Opt=@(t)((initial_volume*420)./(initial_volume+(420-initial_volume)*exp(-
0.1911*t)));
figure(2)
```

```matlab
plot(t,N2_Opt(t));
hold on
plot(1,initial_volume,'*',21,tumor_volume_21,'*',27,tumor_volume_27,'*',35,tu
mor_volume_35,'*');
title('Tumor Volume Growth (Logistic Model)')
ylabel('Tumor volume (mm3)')
xlabel('Time (days)')
legend('Logistic','experimental data');
hold on


%Generalized Logistic Model

a0=[18;0.18];
N3=@(x,xdata)((initial_volume*420)./((initial_volume.^x(1)+(420.^x(1)-
initial_volume.^x(1))*exp(-x(2)*x(1)*xdata)).^(1./x(1))));
[x,resnom] = lsqcurvefit(N3,a0,xdata,ydata)
N3_Opt=@(t)((initial_volume*420)./((initial_volume.^19+(420.^19-
initial_volume.^19)*exp(-0.19*18.2*t)).^(1./19)));
figure(3)
plot(t,N3_Opt(t));
hold on
plot(1,initial_volume,'*',21,tumor_volume_21,'*',27,tumor_volume_27,'*',35,tu
mor_volume_35,'*');
title('Tumor Volume Growth (Generalized Logistic Model)')
ylabel('Tumor volume (mm3)')
xlabel('Time (days)')
legend('Generalized logistic model','Experimental data');
hold on


%Gompertz Model

a0=[0.1;0.02];
N4=@(x,xdata)(initial_volume*exp((x(1)/x(2))*(1-exp(-x(2)*xdata))));
[x,resnom] = lsqcurvefit(N4,a0,xdata,ydata)
alpha=0.25;
betta=0.02;
N4_Opt=@(t)(initial_volume*exp((alpha/betta)*(1-exp(-betta*t))));
figure(4)
plot(t,N4_Opt(t));
hold on
plot(1,initial_volume,'*',21,tumor_volume_21,'*',27,tumor_volume_27,'*',35,tu
mor_volume_35,'*');
title('Tumor Volume Growth (Gompertz)')
ylabel('Tumor volume (mm3)')
xlabel('Time (days)')
legend('Gompertz','Experimental data');
hold on
```

```matlab
% Von Bertalanffy Model

a0=[0.25;0.024;0.9];
N5=@(x,xdata)(((x(1)./x(2))+(initial_volume.^(1-x(3))-(x (1)./x(2)))*exp(-
x(2)*(1-x(3))*xdata)).^(1./(1-x(3)))));
[x,resnom] = lsqcurvefit(N5,a0,xdata,ydata)
a=0.25;
b=0.024;
gamma=0.9;
N5_Opt=@(t)(((a./b)+(initial_volume.^(1-gamma)-(a./b))*exp(-b*(1-
gamma)*t)).^(1./(1-gamma)));
figure(5)
plot(t,N5_Opt(t));
hold on
plot(1,initial_volume,'*',21,tumor_volume_21,'*',27,tumor_volume_27,'*',35,tu
mor_volume_35,'*');
title('Tumor Volume Growth (Von Bertalanffy)')
ylabel('Tumor volume (mm3)')
xlabel('Time (days)')
legend('Von Bertalanffy','Experimental data')
hold on

% Plots

figure(6)
plot(t,N1_Opt(t),t,N2_Opt(t),t,N3_Opt(t),t,N4_Opt(t),t,N5_Opt(t),1,initial_vo
lume,'*',21,tumor_volume_21,'*',27,tumor_volume_27,'*',35,tumor_volume_35,'*'
);
title('Tumor Volume Growth')
ylabel('Tumor volume (mm3)')
xlabel('Time (days)')
legend('Exponential','Logistic','Generalized Logistic','Gompertz','Von
Bertalanffy','Experimental data');
hold on
```

APPENDIX D: MATLAB CODE FOR THE CHEMOTHERAPY EFFECT

MATLAB Code for Mathematical modeling of Glioblastoma volume change under the effect of chemotherapy with F10

```matlab
% MathematicalModelingofGlioblastoma
% NudeMiceIn-vivoModedlWithChemotherapyWithF10

clc;
close all;
format long

% Experimental data

initial_volume=0.26; %mm3
tumor_volume_21=6.34; %mm3 averaged from cage 1
tumor_volume_27=11.232; %mm3 averaged from cage 1
tumor_volume_35=1.044; %mm3 averaged from cage 1

% Variables

xdata=[1 21];
%27 35];
ydata=[0.26 6.34];
%11.8 1.9];
t=linspace(1,35);
t1=linspace(28,35);
t2=linspace(25,35);
t3=linspace(21,35);


% Gompertz Model+chemotherapy effect


a0=[0.25;0.02];
N11=@(x,xdata)(initial_volume*exp((x(1)/x(2))*(1-exp(-x(2)*xdata))));
[x,resnom] = lsqcurvefit(N11,a0,xdata,ydata)
alpha=0.2;
betta=0.02;
N11_Opt=@(t)(initial_volume*exp((alpha/betta)*(1-exp(-betta*t))));
a01=[0.05];
N12=@(x,x1data)(initial_volume*exp((alpha/betta)*(1-exp(-betta*x1data))-
x(1)*((x1data-28))));
[x,resnom] = lsqcurvefit(N12,a01,x1data,y1data)
b=0.25;
N12_Opt=@(t1)(initial_volume*exp((alpha/betta)*(1-exp(-betta*t1))-0.45*(t1-
28)));
N13_Opt=@(t2)(initial_volume*exp((alpha/betta)*(1-exp(-betta*t2))-0.33*(t2-
25)));
```

```matlab
N14_Opt=@(t3)(initial_volume*exp((alpha/betta)*(1-exp(-betta*t3))-0.25*(t3-
21)));
figure(1)
plot(t,N11_Opt(t))
hold on
plot(1,initial_volume,'*',21,tumor_volume_21,'*',27,tumor_volume_27,'*',35,tu
mor_volume_35,'*');
title('Tumor Volume Change')
ylabel('Tumor volume (mm3)')
xlabel('Time (days)')
legend('Gompertz model','Experimental data')
hold on
hold on
figure(2)
plot(t,N11_Opt(t),t3,N14_Opt(t3),t2,N13_Opt(t2),t1,N12_Opt(t1));
hold on
plot(1,initial_volume,'*',21,tumor_volume_21,'*',27,tumor_volume_27,'*',35,tu
mor_volume_35,'*');
title('Tumor Volume Change')
ylabel('Tumor volume (mm3)')
xlabel('Time (days)')
legend('Gompertz model','Day 21','Day 25','Day 28','Experimental data')
hold on
```

APPENDIX E: MATLAB CODE FOR THE SENSITIVITY ANALYSIS

MATLAB Code for Sensitivity analysis

```matlab
% MathematicalModelingofGlioblastoma
% Sensitivity Analysis

clc;
close all;
format long

% Experimental data

initial_volume=0.26; %mm3

% Variables

t=linspace(1,35);

% Gompertz Model sensitivity analysis

alpha=0.2;
betta=0.02;
N11_Opt=@(t)((1/betta)*(1-exp(-
betta*t)).*initial_volume.*exp((alpha/betta).*(1-exp(-betta*t))));
N12_Opt=@(t)(initial_volume.*exp((alpha/betta).*(1-exp(-betta*t))));
N13_Opt=@(t)(((-alpha/(betta^2)).*(1-exp(-betta.*t))+(alpha/betta).*(t.*exp(-
betta.*t))).*initial_volume.*exp((alpha/betta).*(1-exp(-betta*t))));
figure(1)
plot(t,(N11_Opt(t)./N12_Opt(t))*alpha)
hold on
plot(t,(N13_Opt(t)./N12_Opt(t))*betta)
title('Sensitivity plot')
ylabel('Sensivity')
xlabel('Time (days)')
legend('alpha','betta')
hold on

% Gompertz Model sensitivity analysis

t1=linspace(25,35);
alpha=0.2;
betta=0.02;
b=0.25;
N11_Opt=@(t1)(((1/betta)*(1-exp(-betta*t1))-
b*t1).*initial_volume.*exp((alpha/betta).*(1-exp(-betta*t1))-b*t1));
N12_Opt=@(t1)(initial_volume*exp((alpha/betta)*(1-exp(-betta*t1))-b*(t1)));
N13_Opt=@(t1)(((-alpha/(betta^2)).*(1-exp(-
betta.*t1))+(alpha/betta).*(t1.*exp(-
betta.*t1))).*initial_volume.*exp((alpha/betta).*(1-exp(-betta*t1))-b*t1));
```

```
N14_Opt=@(t1)(-t1.*initial_volume.*exp((alpha/betta).*(1-exp(-betta.*t1))-
b.*t1))
figure(2)
plot(t1,(N11_Opt(t1)./N12_Opt(t1))*alpha)
hold on
plot(t1,(N13_Opt(t1)./N12_Opt(t1))*betta)
hold on
plot(t1,(N14_Opt(t1)./N12_Opt(t1))*b)
title('Sensitivity plot')
ylabel('Sensivity')
xlabel('Time (days)')
legend('alpha','betta','b')
hold on
```